A NEW DC-DC CONVERTER FOR FUEL CELL POWERED RESIDENTIAL POWER GENERATION SYSTEMS

by

Rahul Rajiv Sharma

A thesis submitted in partial fulfillment
of the requirements for the degree

of

Master of Science

in

Electrical Engineering

MONTANA STATE UNIVERSITY
Bozeman, Montana

November, 2006

© COPYRIGHT

by

Rahul Rajiv Sharma

2006

All Rights Reserved

APPROVAL

of a thesis submitted by

Rahul Rajiv Sharma

This thesis has been read by each member of the thesis committee and has been found to be satisfactory regarding content, English usage, format, citations, bibliographic style, and consistency, and is ready for submission to the Division of Graduate Education.

Dr. Hongwei Gao
Chair of Committee

Approved for the Department of Electrical & Computer Engineering

Dr. James Peterson
Department Head

Approved for the Division of Graduate Education

Dr. Carl A. Fox
Vice Provost

STATEMENT OF PERMISSION TO USE

In presenting this thesis in partial fulfillment of the requirements for a master's degree at Montana State University, I agree that the Library shall make it available to borrowers under rules of the Library.

If I have indicated my intention to copyright this thesis by including a copyright notice page, copying is allowable only for scholarly purposes, consistent with "fair use" as prescribed in the U.S. Copyright Law. Requests for permission for extended quotation from or reproduction of this thesis in whole or in parts may be granted only by the copyright holder.

Rahul Rajiv Sharma

November, 2006

ACKNOWLEDGEMENTS

I would like to thank my academic advisor Dr. Hongwei Gao for giving me the opportunity to do this work, for his guidance, patience and financial support. Dr. Gao has been a very strong mentor to me these past few years and I have learned immensely from him – not only technically regarding this work, but how to approach work and research in general. His mentoring will influence me far beyond this work. This work was supported by the United States Department of Energy, as a subcontract from Battelle Memorial Institute and Pacific Northwest National Laboratory under Award DE-AC06-76RL01830. I would like to thank the sponsors for the opportunity to work on this project and for the financial support.

I would like to thank Mr. Andy Olson for his time, excellent technical guidance, encouragement and for serving on my thesis committee. His role has been invaluable in the completion of this work. I would like to thank Dr. Robert Gunderson for his mentoring, encouragement, and for serving on my thesis committee. His time and guidance are truly appreciated. I would like to thank the Head of the ECE Department, Dr. James Peterson for his interest in this work, his time and his guidance. I would also like to thank the staff at the ECE department - Sharon, Muriel, Wilma, Allison, Brent and Barbara. My experience at MSU was made richer by my interactions with these people. Their encouragement, understanding, guidance and friendship are deeply appreciated.

Last but furthest from the least, I would like to thank my parents, Rajiv & Gouri Sharma, my sister Rupa Sharma, my invaluable friends and God. Their contributions cannot be put in words, and I cannot thank them enough.

TABLE OF CONTENTS

LIST OF TABLES

LIST OF FIGURES

Figure Page

LIST OF FIGURES (Cont'd)

Figure Page

ABSTRACT

This thesis presents a new topology for an isolated DC-DC converter for low voltage to high voltage conversions at high power. The proposed converter is targeted for use in fuel cell powered residential power generation systems, where low voltage to high voltage conversion at high power (>5KW) and isolation between input and output are required.

Conventional DC-DC converters like forward, half bridge and full bridge for such applications need to have high turn ratio in their power transformers, to enable the high voltage boosting. This high turns ratio of the transformers results in high leakage inductance which reduces the converter's efficiency and increases the difficulty in control.

The proposed converter overcomes this problem by utilizing the leakage inductance for energy conversion instead of considering it as a parasite. This reduces the problems of low efficiency and difficulty of control, caused by the leakage inductance. The need for a separate inductor is also eliminated. Moreover the switching pattern of the FETs of the proposed converter is designed to achieve soft switching, to reduce the switching losses. Simulation results to verify the energy transfer and the closed loop performance of a 550W prototype are presented. Open loop experimental results of a 350W prototype are also presented.

The concept of interleaving of multiple units of the DC-DC converter is proposed. Interleaving enables paralleling multiple units of the converter to achieve a high combined power. This results in using silicon of lower current rating, lowering the sizes of input and output capacitors and reducing the output ripple. Simulations results are presented that verify the concept of interleaving. Preliminary work to implement interleaving of two units of the proposed converter is presented, and future work is recommended.

CHAPTER 1

INTRODUCTION

Objective

The objective of this work was to investigate a new topology for a DC-DC converter for applications that require low voltage to very high voltage conversion at high power, like fuel cell powered residential power generation. The objective also included verification of the principle of operation of the proposed DC-DC converter by simulation and experimental work.

I proposed a novel topology for an isolated converter that utilizes the leakage inductance of the transformer for energy conversion instead of considering it as a parasite, and thus avoiding the problems of low efficiency and difficulty in control. In this manuscript I have detailed my work starting with detailing the topology of the proposed converter, explaining the working of the converter and presenting the verification of the principle of working, by simulation and experimental results.

Background

Increasing global pollution levels and depleting fossil fuel resources have increased concerns and propelled research towards renewable, clean and efficient energy sources. A major focus of this research has been on fuel cells. Fuel cells are being

proposed and implemented in a variety of applications because of their characteristics of being renewable, clean and efficient [1-3].

A fuel cell powered residential power generation system typically consists of a fuel cell stack feeding a power conditioning system that provides regulated AC output voltage. With developments in fuel cell technology for such applications, there is a need to develop affordable and efficient power conditioning technology to make such systems more viable. Concerted efforts are being made by the U.S. Department of Energy and other strategic industrial allies to develop and improve such power conditioning systems [4-5]. This thesis work is a part of this continuing effort, and presents a novel DC-DC converter for such fuel cell powered residential power generation systems.

Fuel Cell

Fuel Cell is a device that converts the chemical energy contained in a fuel, usually oxygen and hydrogen, electrochemically into electrical energy [3]. The byproducts of fuel cell operation usually are water and heat. Thus fuel cells are pollution free, noise free sources of energy.

Fuel cells are an important technology for a potentially wide variety of applications including on-site electric power for households and commercial buildings; supplemental or auxiliary power to support car, truck and aircraft systems; power for personal, mass and commercial transportation [6].

Principle of Working

The basic physical structure of a fuel cell consists of an electrolyte layer in contact with an anode and a cathode on either side. A schematic representation of a unit cell with the reactant/product gases and the ion conduction flow directions through the cell is shown in Figure 1.

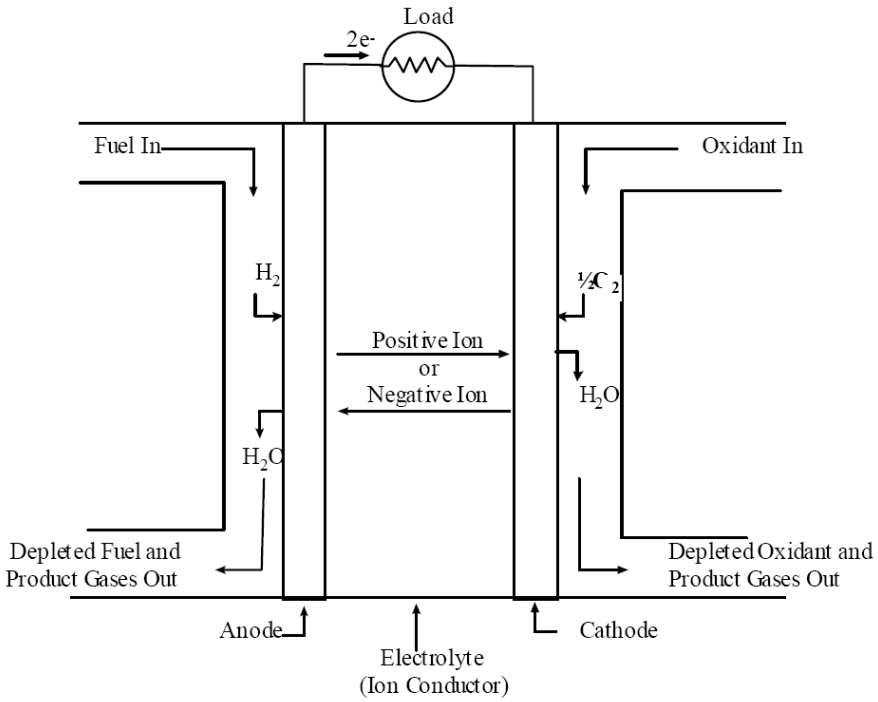

Figure 1. Schematic of a Fuel Cell

Fuel is fed continuously to the anode (negative electrode) and an oxidant (often oxygen from air) is fed continuously to the cathode (positive electrode). The electrochemical reactions take place at the electrodes to produce an electric current through the electrolyte, while driving a complementary electric current that performs work on the load.

Fuel cells run on hydrogen, and so most of fuel cells require a reformer to obtain hydrogen from the hydrocarbon fuels. Fuel cells which operate at high temperatures can run directly on light hydrocarbon fuels such as natural gas or bio-gas. The high temperature at which these fuel cells operate is sufficient to internally reform the hydrocarbons, separating the hydrogen which is then used as fuel [7].

Although a fuel cell is similar to a typical battery in many ways, it differs in several respects. The battery is an energy storage device in which all the energy available is stored within the battery itself. The battery will cease to produce electrical energy when the chemical reactants are consumed i.e. the battery is discharged. A fuel cell, on the other hand, is an energy conversion device to which fuel and oxidant are supplied continuously. In principle, the fuel cell produces power for as long as fuel is supplied.

Most fuel cell systems comprise a number of components:

- Unit cells, in which the electrochemical reactions take place
- Stacks, in which individual cells are modularly combined by electrically connecting the cells to form units with the desired output capacity
- Balance of plant which comprises components that provide feedstream conditioning (including a fuel processor if needed), thermal management, and electric power conditioning among other ancillary and interface functions

Types of Fuel Cells

A variety of fuel cells are in different stages of development. The most common classification of fuel cells is by the type of electrolyte used in the cells and includes 1) Alkaline Fuel Cell (AFC) 2) Polymer Electrolyte Fuel Cell (PEFC) or Proton Exchange

Membrane (PEMFC) 3) Phosphoric Acid Fuel Cell (PAFC) 4) Molten Carbonate Fuel Cell (MCFC) 5) Solid Oxide Fuel Cell (SOFC).

Alkaline Fuel Cell (AFC): Alkaline Fuel Cell is the first modern fuel cell developed in 1960. It has been successfully deployed in many NASA shuttle missions. AFCs use a liquid solution of potassium hydroxide as the electrolyte with a low operating temperature of 70-90 °C. The low operating temperature helps rapid startup of the unit. The sensitivity of the electrolyte to CO_2 necessitates an expensive CO & CO_2 removal system. H_2 is used as the fuel.

Polymer Electrolyte Fuel Cell (PEFC) or Proton Exchange Membrane (PEMFC): This fuel cell technology utilizes a solid ion exchange membrane (fluorinated sulfonic acid polymer or other similar polymer) as the electrolyte. Polymer is an excellent conductor of protons and an insulator of electrons. The only liquid in this fuel cell is water and thus corrosion problems are minimal. Typically, the operating temperature is around 60 to 80 °C. PEFCs are being pursued for a wide variety of applications, especially as for prime power for fuel cell vehicles.

Phosphoric Acid Fuel Cell (PAFC): A liquid phosphoric acid concentrated to 100 percent and contained in a teflon matrix is used as the electrolyte for these fuel cells, which typically operate at 150 to 220 °C. This technology is very tolerant to impurities in the fuel stream and is the most mature in terms of system development and commercialization. PAFCs are mostly developed for stationary applications, and over 200 stationary units with a typical capacity of 200 kW have been installed in the United States.

Molten Carbonate Fuel Cell (MCFC): Usually a molten salt mixture of alkali carbonates is used for the electrolyte, and requires operating temperatures of 600-700 °C where the alkali carbonates form a highly conductive molten salt, with carbonate ions providing ionic conduction. At high operating temperatures, Ni (anode) and nickel oxide (cathode) are adequate to promote reaction. Noble metals are not required for operation, and many common hydrocarbon fuels can be reformed internally. This technology is targeted at medium- and large-scale stationary power generation and marine applications, where the relatively large size and weight of MCFC and slow start-up time are not an issue.

Solid oxide fuel cell (SOFC): A solid nonporous ceramic material is used as the electrolyte at operating temperatures of 600-1000 °C, where ionic conduction by oxygen ions takes place. This high operating temperature, while hampering rapid startup, helps to increase the efficiency and frees up the SOFC to use a variety of fuels without a separate reformer. The high operating temperatures also result in co-generation of usable heat. Thus SOFCs are most suitable for residential power generation. SOFCs are also being used in a variety of other applications including mobile power, auxiliary power for vehicles, and specialty applications.

In parallel with the above classification by electrolyte, some fuel cells are classified by the type of fuel used, which include:

Direct Alcohol Fuel Cells (DAFC) or Direct Methanol Fuel Cells (DMFC): DAFCs use alcohol without reforming. Mostly, this refers to a PEFC-type fuel cell in which methanol or another alcohol is used directly, mainly for portable applications.

Table 1. Comparison of Different Types of Fuel Cells

	PEFC	AFC	PAFC	MCFC	SOFC
Electrolyte	Hydrated Polymeric Ion Exchange Membranes	Mobilized or Immobilized Potassium Hydroxide in asbestos matrix	Immobilized Liquid Phosphoric acid in SiC	Immobilized Liquid Molten Carbonate in $LiAlO_2$	Perovskites (ceramics)
Electrodes	Carbon	Transition metals	Carbon	Nickel and Nickel oxide	Perovskite and Perovskite metal cermet
catalyst	Platinum	Platinum	Platinum	Electrode material	Electrode material
Interconnect	Carbon or metal	Metal	Graphite	Stainless steel or nickel	Nickel, steel or ceramic
Operating Temperature in °C	40 - 80	65 - 220	205	650	600 - 1000
Charge carrier	H^+	OH^-	H^+	$CO3^-$	O^-
Product water management	Evaporative	Evaporative	Evaporative	Gaseous product	Gaseous product
Product heat management	Process Gas + Liquid cooling Medium	Process Gas + Electrolyte Circulation	Process Gas + Liquid Cooling Medium or Steam Generation	Internal Reforming + Process Gas	Internal Reforming + Process Gas

Direct Carbon Fuel Cells (DCFC): In direct carbon fuel cells, solid carbon is used directly in the anode, without an intermediate gasification step. The thermodynamics of the reactions in a DCFC allow very high efficiency conversion.

Fuel Cell V-I Curve

The typical fuel cell V-I curve is shown in Figure 2. It can be seen that with increasing load current, the fuel cell voltage drops by a huge percentage. In this case a typical 42V fuel cell drops down to 22V at 36A load. This is a drop of about 50% in the fuel cell voltage. This shortcoming of the fuel cell has to be compensated for, by external electronic circuitry before the energy can be sourced into any application.

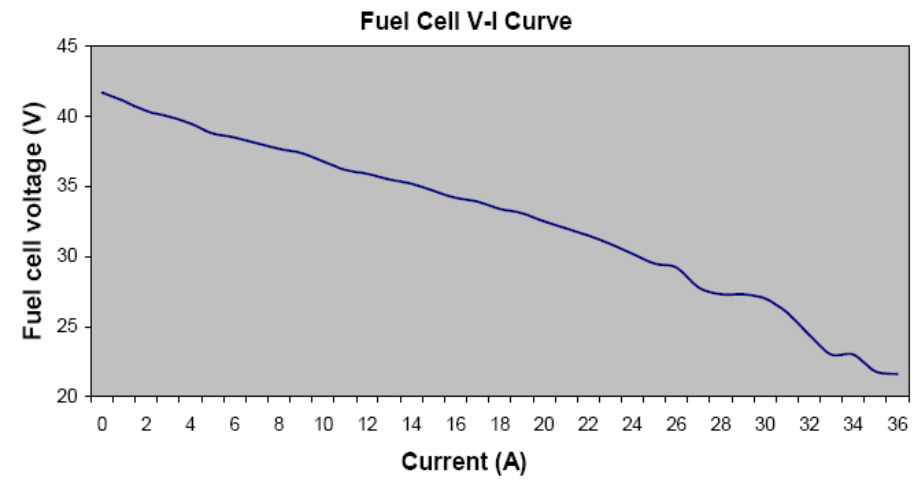

Figure 2. Typical Fuel Cell Voltage / Current Characteristics [8]

Fuel Cell Powered Residential Power Generation System

The configuration of a typical fuel cell powered residential power generation system is shown in Figure 3. The fuel cell voltage is fed into a DC-DC converter to obtain a high voltage, regulated DC link. A battery pack is attached to the DC link to supplement the fuel cell power during periods of high load demand and to compensate for

the slow dynamic response of the fuel cell. Finally a DC/AC inverter, with output filter cascade-connected, is used to obtain split phase AC voltage feeding the load.

The DC voltage generated by a fuel cell stack is low in magnitude (<50V for a 5 to 10kW system, <350V for a 300kW system) [9]. According to the specifications of 2003 International Future Energy Challenge for such an application, the fuel cell output voltage is 22V-41V and the AC load is 120/240V at 5kW continuous and 10kW peak. The fuel cell is rated for an output of 5kW and is supplemented by a 5kW battery pack [10]. The DC-DC converter is therefore required to boost the low fuel cell voltage to a regulated higher voltage DC (400V typical for 120/240V AC output), while also electrically isolating its input from its output.

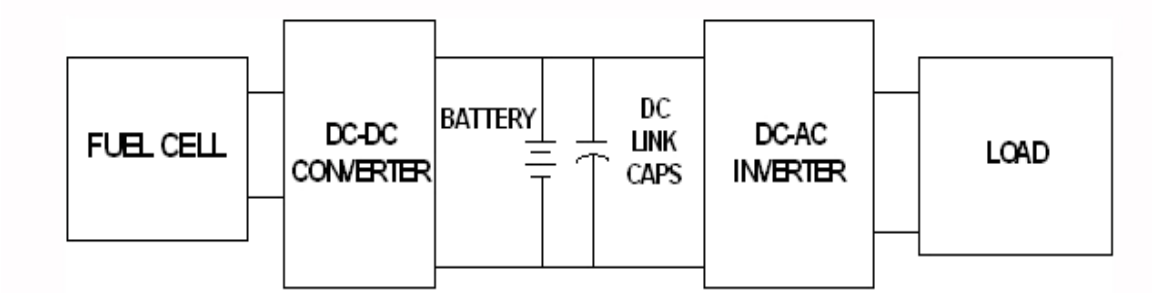

Figure 3. Typical Fuel Cell Powered Residential Power Generation System

Overview of Conventional Isolated DC-DC Converters

The basic principle of working of isolated DC-DC converters consists of switching the input DC voltage at high frequency to form a high frequency AC voltage. This AC voltage is applied across the primary of a transformer, with appropriate primary and secondary turns to step up or step down the AC voltage to the desired level. The high frequency of the AC voltage enables a considerable reduction of the size of the

transformer, as compared to a transformer operating at line frequency (50/60Hz). The AC voltage at the secondary of the transformer is then rectified to obtain unfiltered DC voltage. This voltage is then filtered using a capacitive filter, to provide the desired DC output voltage [11].

A number of existing conventional isolated DC-DC converters can be considered as candidates for a fuel cell powered residential power generation system. These conventional isolated DC-DC converters are forward, push-pull, half bridge and full bridge [12-16]. Figure 4 shows the schematics of these conventional isolated converters.

Forward converter has the drawback of limited duty cycle, and thus is unsuitable for high power applications. Moreover the switch in the forward converter has to be rated for twice the input voltage. The push-pull converter's problem is the center tap termination, which tends to cause saturation of the transformer at high power levels due to slightly unbalanced excitation [17]. The half-bridge topology can be used, but it requires a split capacitor bus, twice the device current, and twice the transformer turn ratio [18]. Apart from these problems, all these converters have problems of difficulty in control and lowered efficiency due to high leakage inductance of their transformers in high voltage boosting applications, like fuel cell powered residential power generation.

The full-bridge topology works well and is the most commonly used topology for high power applications. The voltage and current stresses on the switches are the least on a full bridge converter. However the problems caused by high leakage inductance still exist in the full bridge converter.

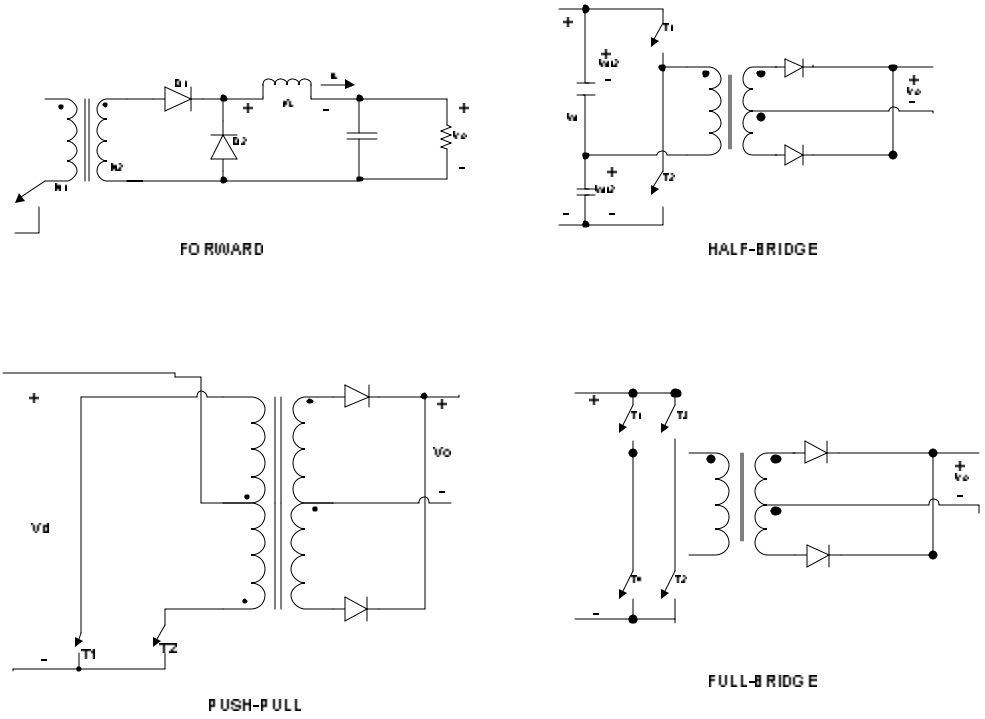

Figure 4. Conventional Isolated DC-DC Converters

Table 2. Comparison of Conventional Isolated DC-DC Converters [14]

Topology	Number of Switches	Device Voltage Rating (V_S = Supply Voltage)	Notes
Forward	1	$2V_S$	Requires lossy resetting, limited duty cycle
Push-Pull	2	$2V_S$	Center tap of transformer is problem at high power
Half-bridge	2	V_S	Requires twice device current
Full-bridge	4	V_S	Smallest current and voltage stresses on devices

In this work a new DC-DC converter which addresses these problems of conventional DC-DC converters is proposed. The proposed converter utilizes the leakage inductance of the transformer for energy conversion instead of considering it as a parasite. This reduces the problems of low efficiency and difficulty of control. Moreover *soft switching* technique is employed to reduce the switching losses.

Soft Switching

During the switching interval, there is a finite period as the transistor begins to conduct where the voltage begins to fall at the same time as current begins to flow. This simultaneous presence of voltage across the transistor and current through it means that, during this period, high power is being dissipated within the device. A similar event occurs as the transistor turns off, with the full current flowing through it. This kind of switching is called hard switching. If the switching period is reduced through the use of improved driving circuitry, the faster rise and fall times generate more high frequency energy that is radiated and conducted out of the unit as unacceptable Radio Frequency Interference (RFI). If the rise and fall times are intentionally slowed to reduce the RFI, the power losses in the transistor increase proportionally, increasing the thermal stress on the part, thus reducing its lifespan. To avoid these problems caused by hard switching, soft switching is employed in switching power converters. In soft switching the voltage across each transistor is allowed to swing to zero before the device turns on and current flows. Not only does soft switching generate significantly less electrical noise, it achieves greater efficiency, longer mean time between failures (MTBF), and higher immunity to the effects of other equipment operating nearby [19-20].

CHAPTER 2

PROPOSED DC-DC CONVERTER

Topology

Figure 5 shows the topology of the proposed converter, where FC is the low voltage (22-41V) fuel cell; S1-S6 are active switches; D1-D6 are body diodes of switches S1-S6 respectively; D7 and D8 are power diodes; C is the filter capacitor; T is the transformer; R is the load of the DC-DC converter.

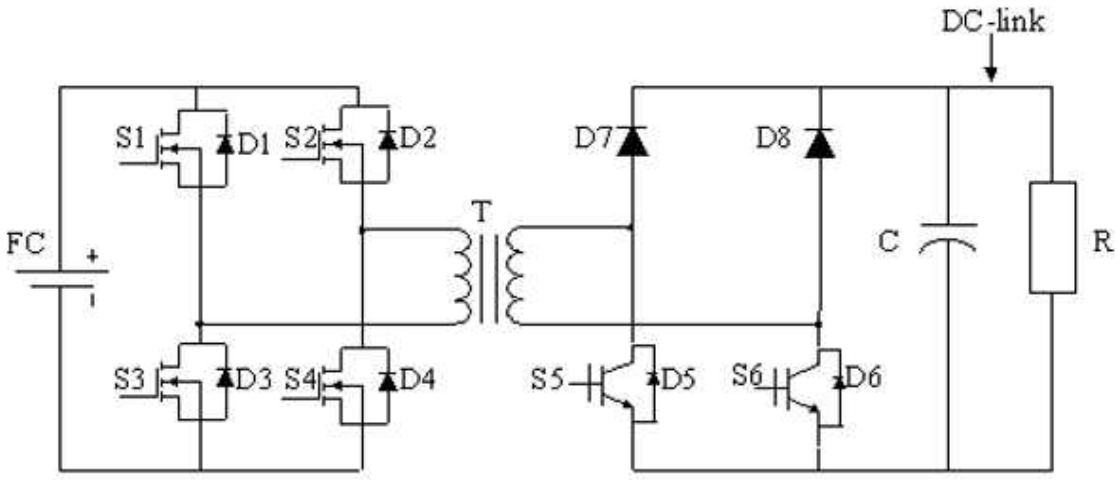

Figure 5. Topology of the Proposed DC/DC Converter

Working

The transformer primary side referred equivalent circuits of the converter are shown in Figure 6 and are used to explain the operation of the converter. The

magnetizing inductance of the transformer is ignored and only the leakage inductance is considered in the derivation of the equivalent circuits. The waveforms of key components of the converter in one complete cycle are shown in Figure 7. In Figure 6, and Figure 7, V_I, V_O, V_P, V_S, V_L, and I_L stand for the input voltage of the converter, output voltage of the converter, primary side voltage of the transformer, secondary side voltage of the transformer (primary side referred), voltage across the leakage inductance of the transformer (primary side referred), and primary side current of the transformer, respectively. In Figure 7, G1-G6 represent the gating signals to switches S1-S6 respectively and the time period from t0-t8 represents a complete operating cycle of the converter. As shown in Figure 7, the operation of the converter in the second half cycle, from t4-t8, is similar to that in the first half cycle, from t0-t4, except being in the opposite direction. Therefore, only the operation of the converter in the first half cycle, from t0-t4, is detailed and illustrated in Figs. 6a-6.d.

The operation of the converter during different time periods in the first half cycle is explained as follows.

[t0-t1]: Switches S2, S3, and S5 are gated. A closed current path is created through the fuel cell, S2, the leakage inductor of the transformer, S5, D6, and S3, as shown in Fig. 3.a. As a result, one can have:

$$V_P = V_I \tag{1}$$

$$V_S = 0 \tag{2}$$

and therefore,

$$V_L = V_P - V_S = V_I - 0 = V_I \tag{3}$$

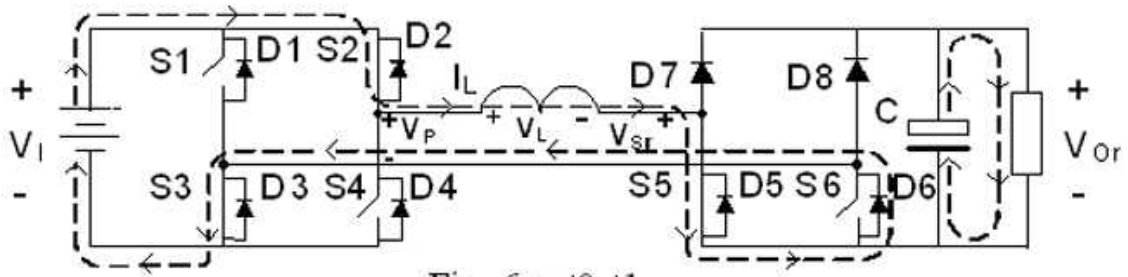

Fig. 6.a t0-t1

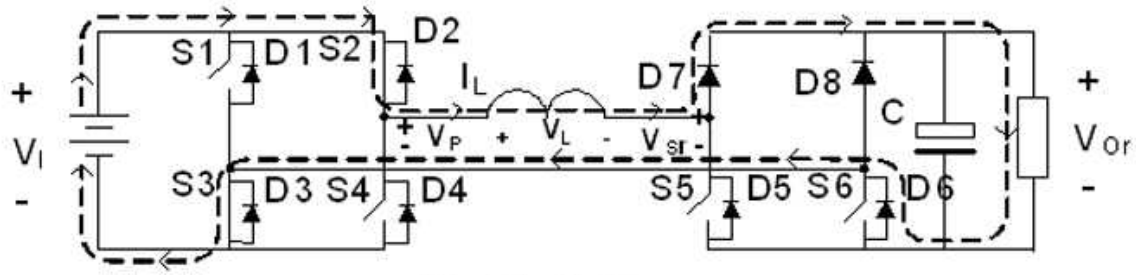

Fig. 6.b t1-t2

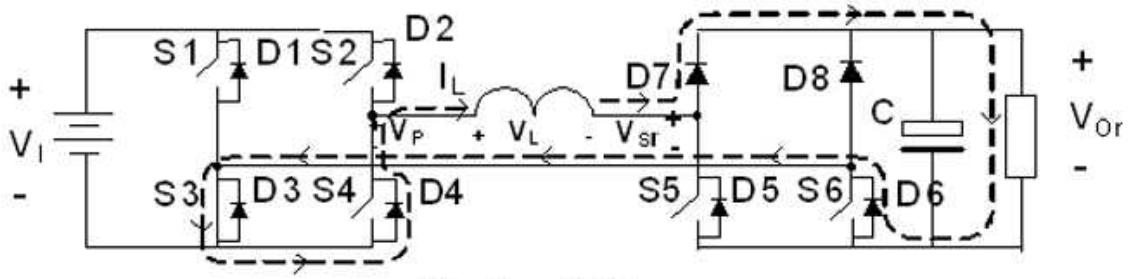

Fig. 6.c t2-t3

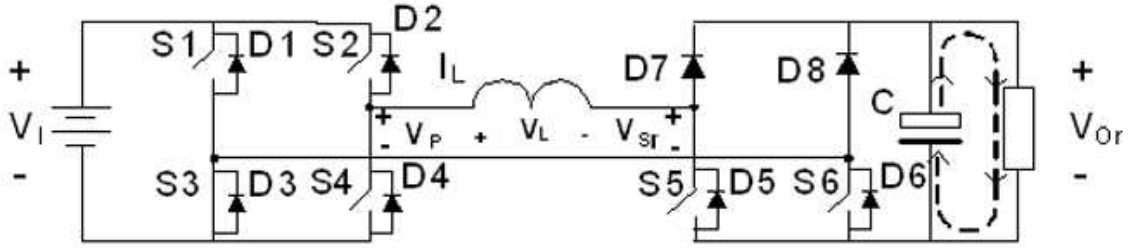

Fig. 6.d t3-t4

Figure 6. Transformer Primary Side Referred Equivalent Circuits of the Converter During Different Time Periods in the First Half Cycle

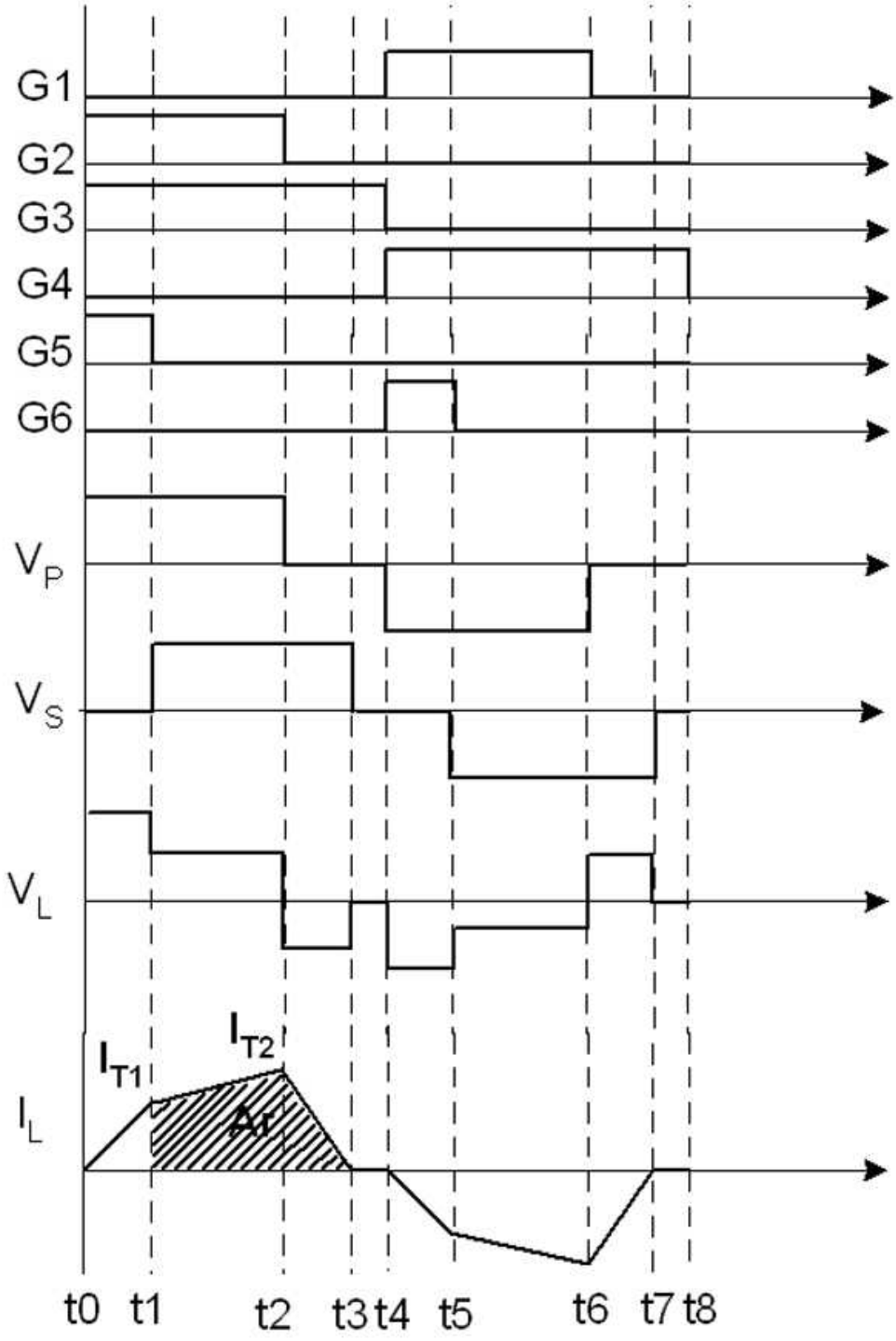

Figure 7. Waveforms of Key Components of the Converter in One Complete Cycle

The current through the leakage inductance is given by:

$$I_L(t) = \frac{1}{L}\int_{t0}^{t} V_L\,dt + I_{t0} \tag{4}$$

Where, I_{t0} is the inductor current at the moment t=t0, which equals zero and L is the leakage inductance of the transformer (primary side referred). Substituting (3) and I_{t0}=0 into (4) yields:

$$I_L(t) = \frac{1}{L}V_I t \tag{5}$$

It can be seen from (5) that the inductor current ramps up linearly from zero due to the positive constant V_I, as shown in Fig. 4. The energy flow during this period is from the fuel cell to the leakage inductor of the transformer and the filter capacitor to the load. One can also see that switches S2, S3, and S5 are turned on at zero current condition at the moment t0.

Substituting t=T_1 into (5), Where T_1 is the time period from t0 to t1 as shown in Fig. 4, one can solve the inductor current at time instant t1, I_{T1}, as:

$$I_{T1} = \frac{V_I T_1}{L} \tag{6}$$

[t1-t2]: Switches S2 and S3 are kept on while switch S5 is turned off. D7 conducts to carry the inductor current as a result of the turn-off of S5. A closed current path is created through the fuel cell, S2, the leakage inductor of the transformer, D7, the load and the filter capacitor, D6, and S3. As a result, one can have:

$$V_P = V_I \tag{7}$$

$$V_S = V_O \tag{8}$$

and therefore,

$$V_L = V_P - V_S = V_I - V_O \tag{9}$$

In this work, V_O is controlled to be lower than V_I. Therefore, V_L is still positive but decreases from it previous value.

The current through the leakage inductance is given by:

$$I_L(t) = \frac{1}{L}\int_{t1}^{t} V_L\,dt + I_{T1} \tag{10}$$

Substituting (6) and (9) in (10), one can have:

$$I_L(t) = \frac{1}{L}(V_I - V_O)t + \frac{V_I T_1}{L} \tag{11}$$

It can be seen from (11) that the inductor current still has a linear relationship with time and continues to rise, but now at a slower rate due to the reduced voltage applied to the inductor, as shown in Fig. 4. The flow of energy during this time period is from the fuel cell to the leakage inductor, the filter capacitor, and the load.

Substituting $t=T_2$ into (11), where T_2 is the time period from t1 to t2, one can solve the inductor current at time instant t2, I_{T2}, as:

$$I_{T2} = \frac{(V_I - Vo)T_2}{L} + \frac{V_I T_1}{L} \tag{12}$$

[t2-t3]: Switch S2 is turned off while S3 is kept on. D4 conducts to carry the inductor current as a result of the turn-off of S2. The inductor current flows through D7, the load and the filter capacitor, D6, S3, and D4. As a result, one can have:

$$V_P = 0 \tag{13}$$

$$V_S = V_O \tag{14}$$

and therefore,

$$V_L = V_P - V_S = -V_O \tag{15}$$

The current through the leakage inductance is given by:

$$I_L(t) = \frac{1}{L}\int_{t2}^{t} V_L\,dt + I_{T2} \tag{16}$$

Substituting (12) and (15) into (16) yields:

$$I_L(t) = \frac{1}{L}(-V_o)t + \frac{(V_I - V_O)T_2}{L} + \frac{V_I T_1}{L} \tag{17}$$

It can be seen from (17) that the inductor current still has a linear relationship with time, but due to the negative voltage across the leakage inductance it now decreases linearly with time, until it becomes zero at time instant t3 as shown in Fig. 4. The flow of energy during this period is from the leakage inductor to the filter capacitor and the load.

Since

$$V_L = -Vo = L\frac{di}{dt} = -\frac{LI_{T2}}{T_3} \tag{18}$$

Where T_3 is the time period from t2 to t3, T_3 can be give as:

$$T_3 = \frac{LI_{T2}}{V_O} \tag{19}$$

Substituting (12) into (19) yields:

$$T_3 = \frac{(V_I - Vo)T_2}{V_O} + \frac{V_I T_1}{V_O} \tag{20}$$

Equation (20) shows the dependence of T_3 on T_1 and T_2 under given converter input and output voltage.

[t3-t4]: No current or energy flow in the converter. S3 is turned off at t=t4. It should be noted that S3 is turned off at zero current condition.

From the explanation of the working of the proposed converter one can see that the proposed DC-DC converter does not have energy circulation problem and soft switching is achieved for power switches.

Analytical Derivations and Relations

The waveform of the output current is the waveform outlining the shaded area (Ar) in Fig. 7, diminished by a factor n (transformer turns ratio). The average output current is given as:

$$I_{O\,avg} = \frac{Ar}{nT/2} \tag{21}$$

Where T is the time period of one complete operating cycle of the converter.

It can be seen clearly in Fig. 7 that Ar is equal to the sum of the area of the trapezoid formed by I_{T1} and I_{T2} as parallel sides and the area of the right angled triangle formed with T3 and I_{T2} as the base and the height. Thus Ar is given as:

$$Ar = \frac{1}{2}(I_{T1} + I_{T2})T_2 + \frac{1}{2} I_{T2} T_3 \tag{22}$$

Substituting (6) and (12) into (22) yields:

$$Ar = \frac{\left[(V_I - V_O)T_2 + 2V_I T_1\right]T_2 + \frac{\left[(V_I - V_O)T_2 + V_I T_1\right]^2}{V_o}}{2L} \tag{23}$$

Substituting (23) into (21), one can have:

$$I_{O\,avg} = \frac{\left[(V_I - V_O)T_2 + 2V_I T_1\right]T_2 + \frac{\left[(V_{Ii} - V_O)T_2 + V_{Ii}T_1\right]^2}{V_o}}{nLT} \qquad (24)$$

It can be seen from (24) that the average output current and hence the power of the converter can be controlled by controlling T1 and T_2.

Control Scheme

This section details the control scheme used to control T1 and T2 and hence the power of the proposed converter. A brief background and advantages of the control methods used is also given.

Figure 8 shows the block diagram representation of the control scheme of the proposed converter. The output voltage of the converter is sensed using a voltage divider resistor circuit and the representative signal is compared to a preset reference voltage. The resultant signal is fed into a *Proportional Integral (PI)* circuit resulting in the reference output current signal. This signal is compared to the sensed output current and the resultant signal is fed into two different PI circuits, to obtain signals corresponding to time periods T1 and T2. These signals are compared to a high frequency saw tooth signal to generate appropriate PWM control signals. The PWM control signal corresponding to time period T/2 is generated by comparing a preset fixed value signal to the high frequency saw tooth signal.

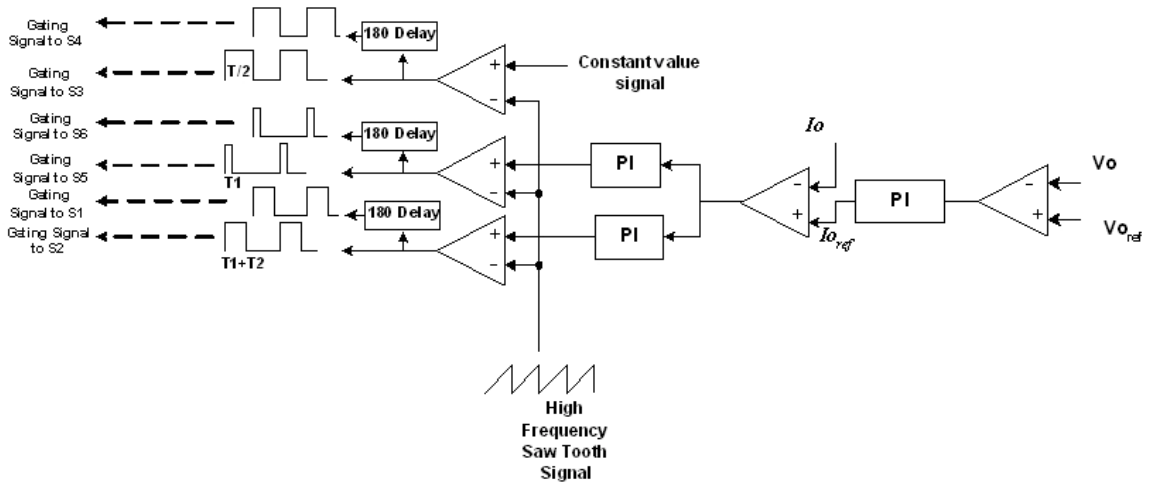

Figure 8**.** Control Scheme of Proposed Converter

Background and Advantages

Pulse Width Modulation. In general switching converters can be controlled by

a) varying the frequency of switching, while keeping the on and off time durations constant

b) varying the on and off time durations of the switch while keeping the frequency of switching constant

c) varying both the on and off durations of the switch as well as the frequency of switching.

Variation in the switching frequency makes it difficult to filter the ripple components in the input and output waveforms of the converter. Thus methods involving frequency variations are not commonly used. The most common method of controlling the on and off time durations of the switches in a power converter is called *Pulse Width Modulation (PWM)* [21]. In the PWM control scheme, the switch control signal, which

controls the on or off state of the switch, is generated by comparing a signal-level control voltage $v_{control}$ with a repetitive waveform as shown in Figure 9.

The control voltage signal generally is obtained by amplifying the error, or the difference between the actual output voltage and its desired value. The frequency of the repetitive waveform with a constant peak, which is shown to be a saw tooth, establishes the switching frequency. This frequency is kept constant in a PWM control and is chosen to be in a few kilohertz to a few hundred kilohertz range. When the amplified error signal, which varies very slowly with time relative to the switching frequency, is greater than the saw tooth waveform, the switch control signal becomes high, causing the switch to turn on. Otherwise the switch is off [22]. In terms of $v_{control}$ and the peak of the saw tooth waveform V_{st} in figure, the switch *duty ratio* can be expressed as

$$D = \frac{t_{on}}{T_s} = \frac{v_{control}}{Vst} \tag{31}$$

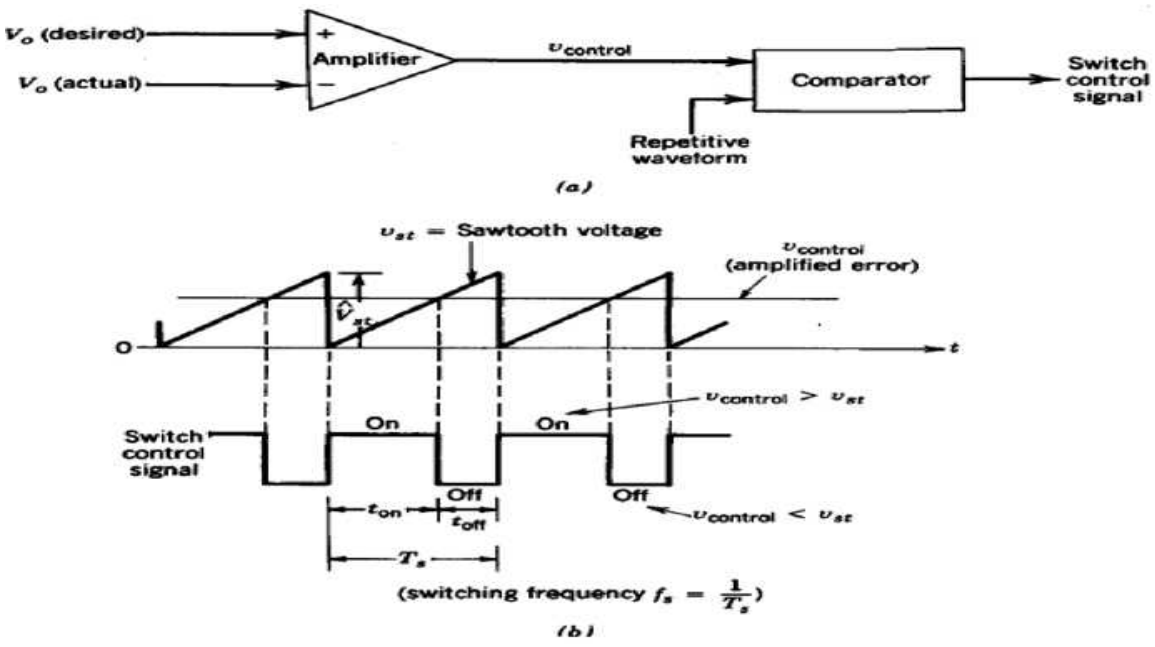

Figure 9. Pulse-Width Modulator: (a) Block Diagram, (b) Comparator Signals

PI Control. The feedback loop of the proposed converter is implemented in the simulation using Proportional Integral (PI) control method. The PI feedback control method adds positive corrections, removing the error from a system's controllable variable as shown in Figure 10. PI feedback control method consists of two actions – the *proportional* action and the *integral* action. The proportional action involves multiplying the error with a negative constant (proportional gain) and adding the product to the controlled quantity. The principle of proportional action requires that the amount of change in the manipulated variable vary directly with the size of the error i.e. the proportional gain dictates the sensitivity of the corrective action. The integral action involves integrating the error over a period of time and then multiplying with a negative constant (integral gain) and adding the product to the controlled quantity. Therefore this action averages the measured error over a period of time to find the process output's average error from the desired value. Integral action brings the controlled variable back to the set point in the presence of a sustained upset or disturbance i.e. integral action acts to eliminate steady state error [23].

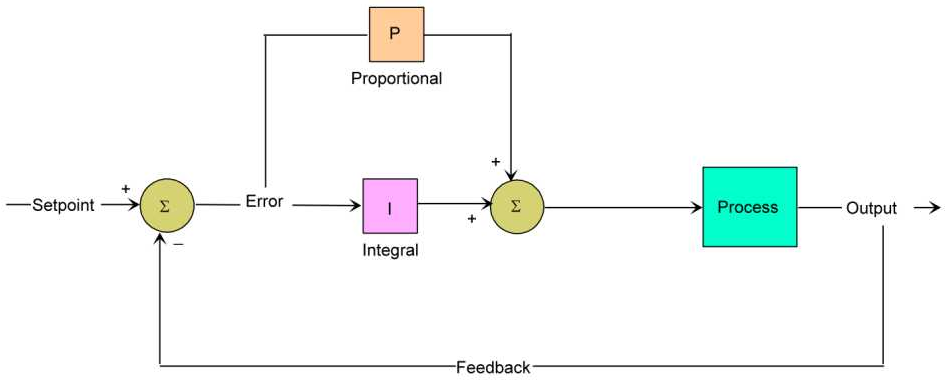

Figure 10. PI Control Scheme [19]

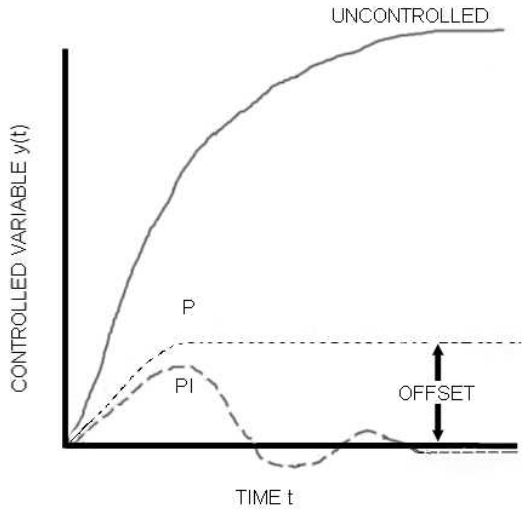

Figure 11. Need for PI Control [23]

A simple proportional system either oscillates, moving back and forth around the setpoint because there's nothing to remove the error when it overshoots, or oscillates and/or stabilizes at a too low or too high value. By adding a negative proportion of (i.e. subtracting part of) the average error from the process input, the average difference between the process output and the setpoint is always being reduced. Thus ultimately the output of a PI controlled system settles down at the desired value.

Table 3. Effect of Increasing the Proportional and Integral Gains on Different Response Characteristics of a System [23]

Parameter	Rise Time	Overshoot	Settling Time	Steady state error
P	Decrease	Increase	Small change	Decrease
I	Decrease	Increase	Increase	Eliminate

Essentially proportional control produces steady state error; integral control corrects the steady state error but it degrades transient response. Combining instantaneous response characteristics of proportional control with the zero steady state characteristic of integral control results in a system with low steady state error and fast transient response [23].

PI control does not require knowledge of the value of the leakage inductance, and therefore is the choice of control for the proposed converter. Moreover PI control also eliminates the need for a separate sensor to measure the input voltage.

CHAPTER 3

VERIFICATION

This chapter describes the verification of the proposed DC-DC converter by simulation of a 550W unit and with experimental results of a 350W prototype.

Simulation

Simulation of the proposed converter was performed in PSIM; a commercial simulation tool specifically designed for power electronics. Performance of the proposed converter was simulated for the full load power of 550W; fuel cell input voltage 21-42V and output voltage 350V. The fuel cell input voltage was simulated using a simplified electrical equivalent model [15], which emulates the typical V-I characteristics of a fuel cell as described earlier in Chapter 1.

Figure 12 shows the schematic of the simulation model as seen in the PSIM interface. The simplified fuel cell equivalent electrical model consists of a resistance in series with a constant voltage source. The voltage drop across the resistance increases, with increasing current and the resistance value is designed to closely emulate the typical fuel cell V-I characteristic. The power transformer was designed with a primary to secondary turns ratio of 1:14 and a primary side referred leakage inductance of 0.1uH. MOSFETs were chosen as the active power switches, as they are the most efficient and economical choice amongst active power switches for this kind of an application. The

switching frequency is chosen as 50 KHz., as it is a nominal common value for switched power converters, which works optimally in terms of the semiconductor losses, and transformer design.

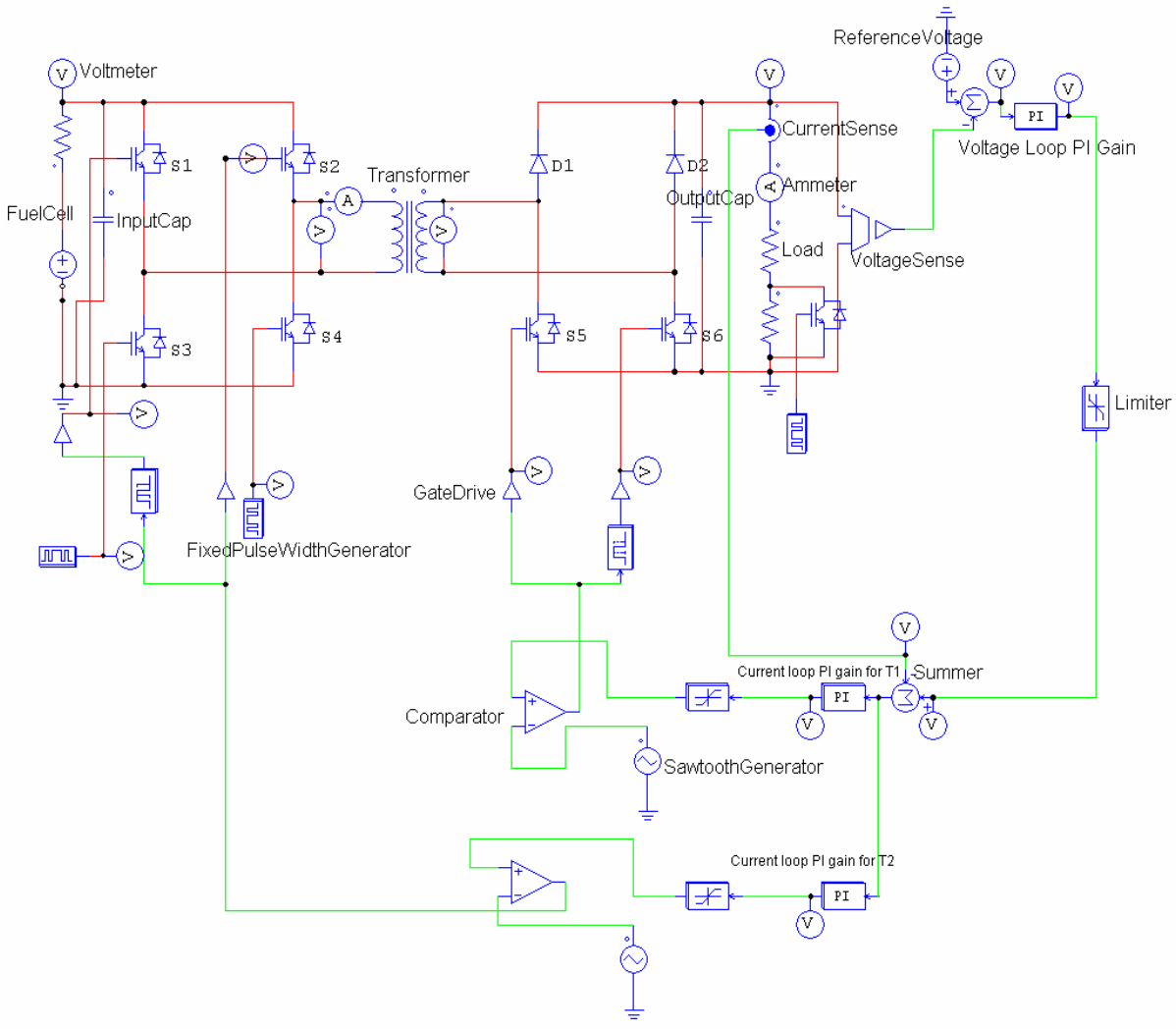

Figure 12. Simulation Schematic of the Proposed Converter

Simulation Results

The simulation schematic is shown in Figure 12. The simulation is run for 700ms with a time step of 0.02us to obtain high resolution waveforms. The results are shown in Figure 13, where from top to bottom are gating signal (G2) of switch S2, gating signal (G3) of switch S3, gating signal (G5) of switch S5, primary side voltage(VP), secondary side voltage (VS), and transformer primary current (I(L)). By comparing the simulation results with the desired waveforms shown in Figure 11, it can be seen that the simulation confirms the designed energy transfer scheme. During time period T1, all switches S2, S3 and S5 are on, VP is positive and Vs =0. Thus the current through the transformer rises linearly. During time period T2, S5 is turned off and S3 and S3 are kept on. Both VP and VS are positive, but VP >Vsr, where Vsr is the secondary side voltage referred to the primary side. Therefore, the current through the transformer continues to rise, but at a very slow rate (because of small difference between VP and Vsr). During time period T3, switch S2 is switched off and only switch S3 is on. Now Vs is positive and VP=0. The transformer current starts to fall and falls till it reaches zero. During time period T4, all three switches are off, VP and Vs both are zero, and there is no current through the transformer.

The closed-loop performance of the proposed converter is also investigated by the simulation. The PI parameters are manually tuned to get small rise time, settling time, overshoot and steady state error as seen in Figure 14. The tuning procedure of the PI parameters is started with choosing a low proportional gain and zero integral gain for all the controllers. It is kept in mind that the proportional gains for the two controllers for

generating signals corresponding to T1 and T2, need to have a ratio of about 1:10 respectively. Also it is kept in mind that the final control signals with a gain comprising of the product of the two gains of the voltage loop and the current loop, are finally compared to a sawtooth waveform of amplitude 0.5V peak-peak to generate the PWM signals. The proportional gains are increased in this proportion till the response time is as fast as possible without increasing the overshoot by over about 20%. The integral gain is then increased to reduce the overshoot to less than 10%. Also since the current loops have to be faster than the voltage loop, the integral gain of the current loops is kept smaller than the voltage loop. The parameters are then fine tuned and the final PI parameters for the voltage loop and the two current loops used in the simulation are given in Table 4.

Table 4. PI Gain Values for All the Controllers in the Feedback Loop

Controller	Proportional Gain	Integral Gain (Time Constant in Seconds)
Voltage Loop	0.04	0.01
Current Loop for T1	0.01	0.001
Current Loop for T2	0.001	0.001

Before t=0.25 s, the converter is in a stable state with the output voltage at 350V and the output current equal to 0.95Amps. The fuel cell voltage is 35V and the fuel cell current is 10 Amps. At time instant t=0.25s the load current is stepped up by 50%, to 1.5Amps. It can be seen that the output voltage is maintained at 350V after a small dip. The fuel cell voltage drops from 35V to 26V as the fuel cell current increases from 10

Amps to 21Amps. At time instant t=0.5s, the output current is stepped down to its original value of 0.95Amps, and it is seen that the output voltage again maintains at 350V, after a small shoot up. The fuel cell voltage rises back from 26V to 35V as the fuel cell current falls from 21 Amps back to 10 Amps. It is therefore verified by simulation that the proposed converter can maintain designed output voltage under varying loads.

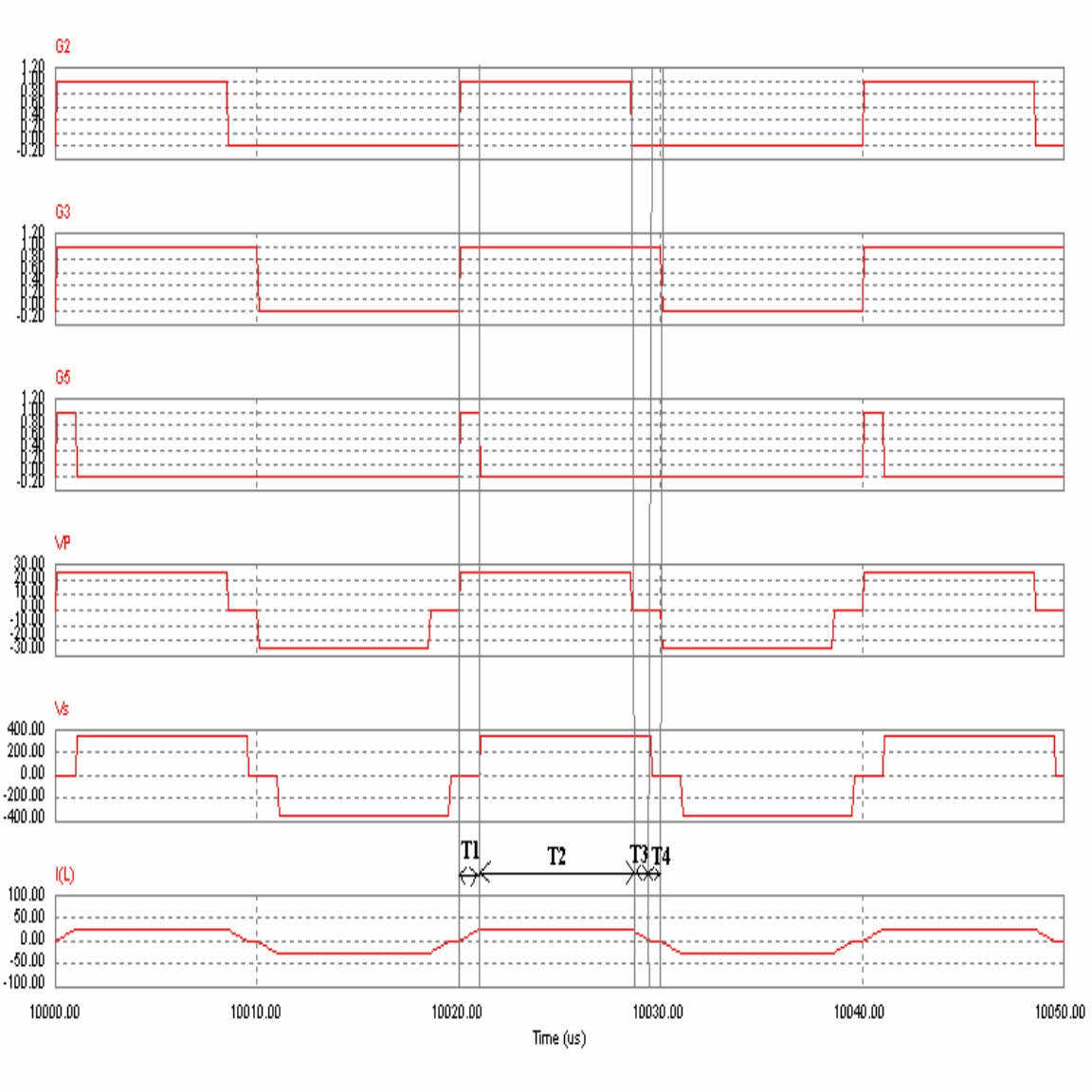

Figure 13. From Top to Bottom Open Loop Simulation Results of Gating Signal of Switch S2, Gating Signal of Switch S3, Gating Signal of Switch S5, Primary Side Voltage, Secondary Side Voltage, and Transformer Primary Current

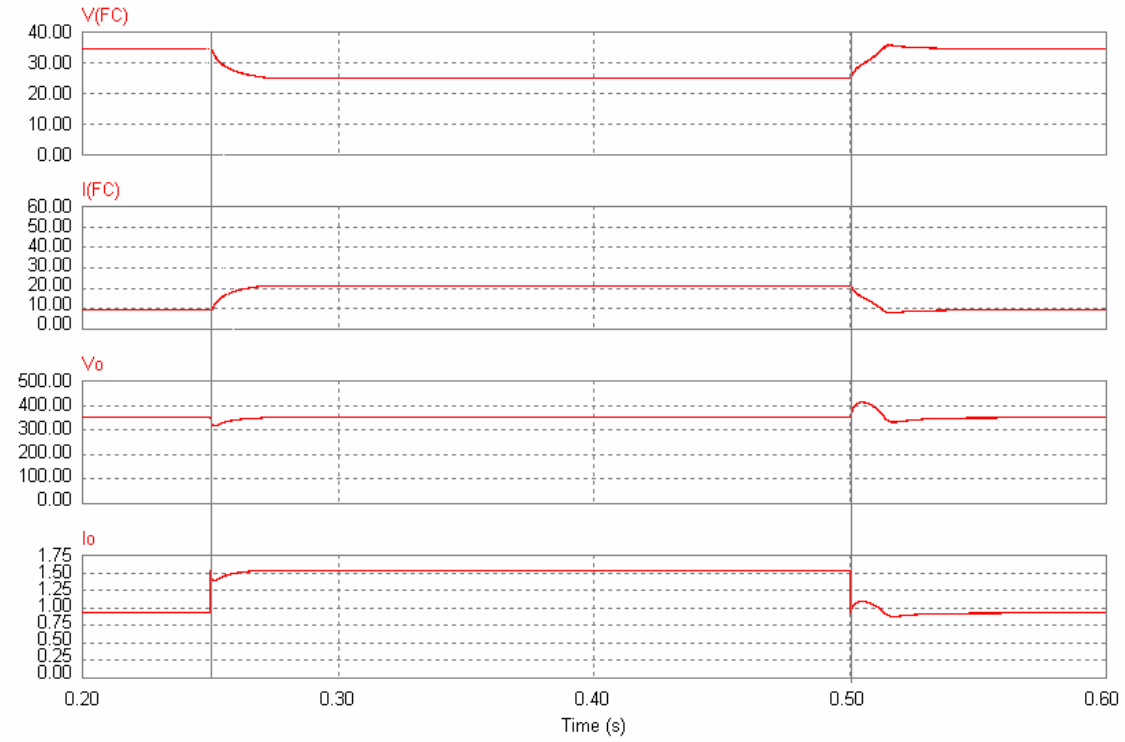

Figure 14. Simulated Closed Loop Behavior

Experimental Setup

Open loop experimental verification of the proposed converter was performed in the laboratory. Figure 15 shows the basic layout of the laboratory setup. A 350W prototype of the proposed converter was built in the laboratory. A 35V/20A power supply was used as the source of power for the setup. A DSP chip (TMS320LM2407A) by Texas Instruments was used to generate constant value PWM control signals, which were fed into a gate drive circuit board using IR2120 integrated gate drivers that drove the MOSFETs. A bank of high power resistors were used as the load. A digital oscilloscope was used to obtain waveforms.

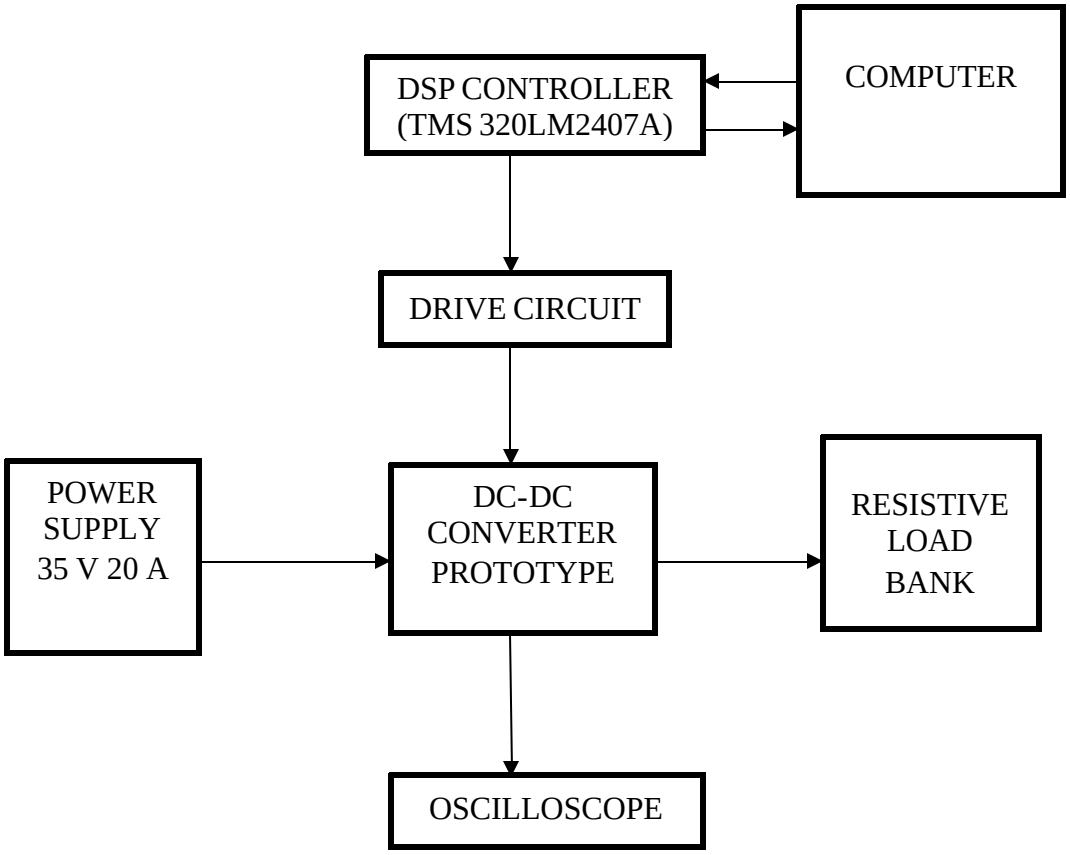

Figure 15. Laboratory Setup Schematic of 350W Prototype

The prototype was successfully tested and it provided a DC output voltage of 350V, for an input voltage of 25V at 350W. The waveforms of the voltage of the primary side of the transformer, the voltage of the secondary side of the transformer and the current through the primary side of the transformer as obtained experimentally are shown in Figure 16. It can be seen that the transformer primary current waveform conforms to the designed transformer current waveshape in Figure 7. Both the primary side current and the secondary side current waveforms through the transformer, could not be recorded simultaneously as the laboratory only had one current probe. The secondary side transformer current is thus not shown in Figure 16, but during the work it was confirmed

that the transformer secondary current also had the same waveshape as the transformer primary side current, with the amplitude diminished by the turns ratio. The primary side voltage and secondary side voltage waveforms of the transformer also conform to the desired waveshape shown in Figure 7. The amplitudes of the primary side voltage and secondary side voltage of the transformer, and the current through the transformer show that the converter is operating at 350W. The energy transfer principle of the proposed DC-DC converter is thus verified.

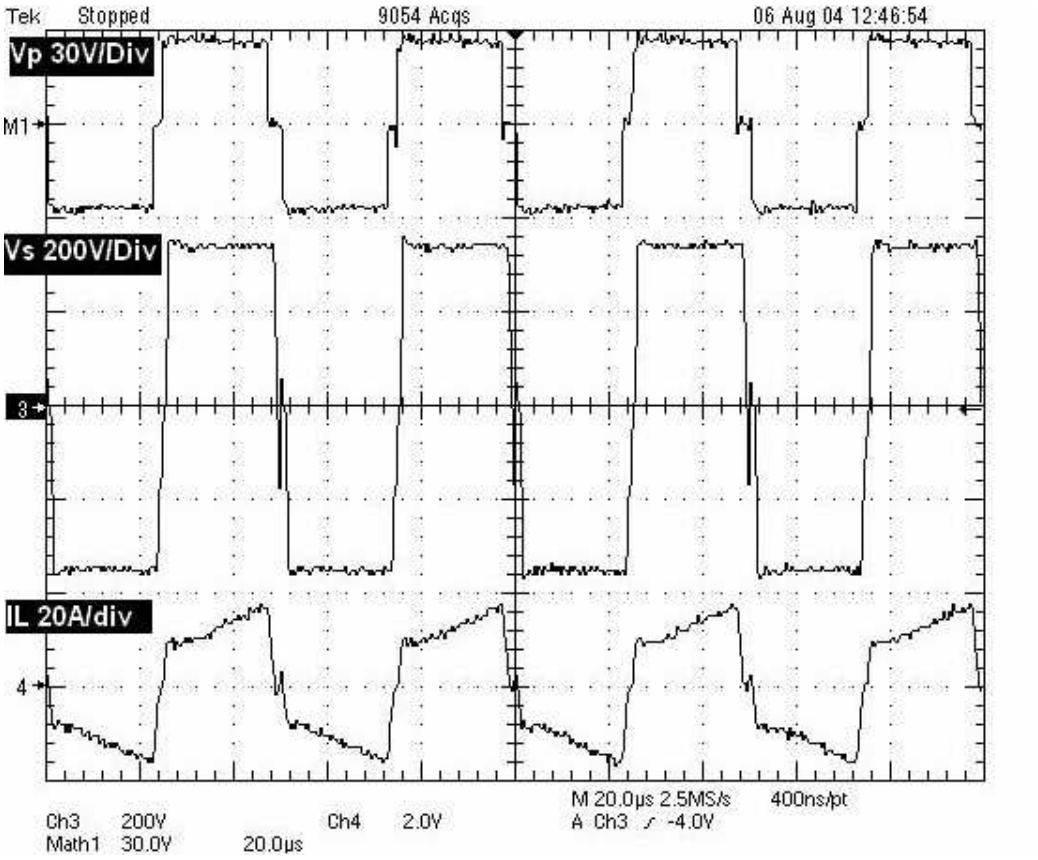

Figure 16. From Top to Bottom: Experimental Recorded Voltage of the Primary Side of the Transformer (30V/div), Voltage of the Secondary Side of the Transformer (200V/div), and Current of the Primary Side of the Transformer (20A/div), with a Time Base of 20us/div

The voltages across the MOSFETs and diodes as obtained experimentally are also shown in Figure 17, Figure 18 and Figure 19. The voltage across the upper and lower MOSFETs of the same leg in the primary side are shown in Figure 17. These MOSFETS are rated for 80V, and it can be seen in that the maximum voltage spike is 40V. Thus MOSFETs of lower voltage ratings like 60V can be chosen, which would have lower on resistance and therefore lower conduction losses.

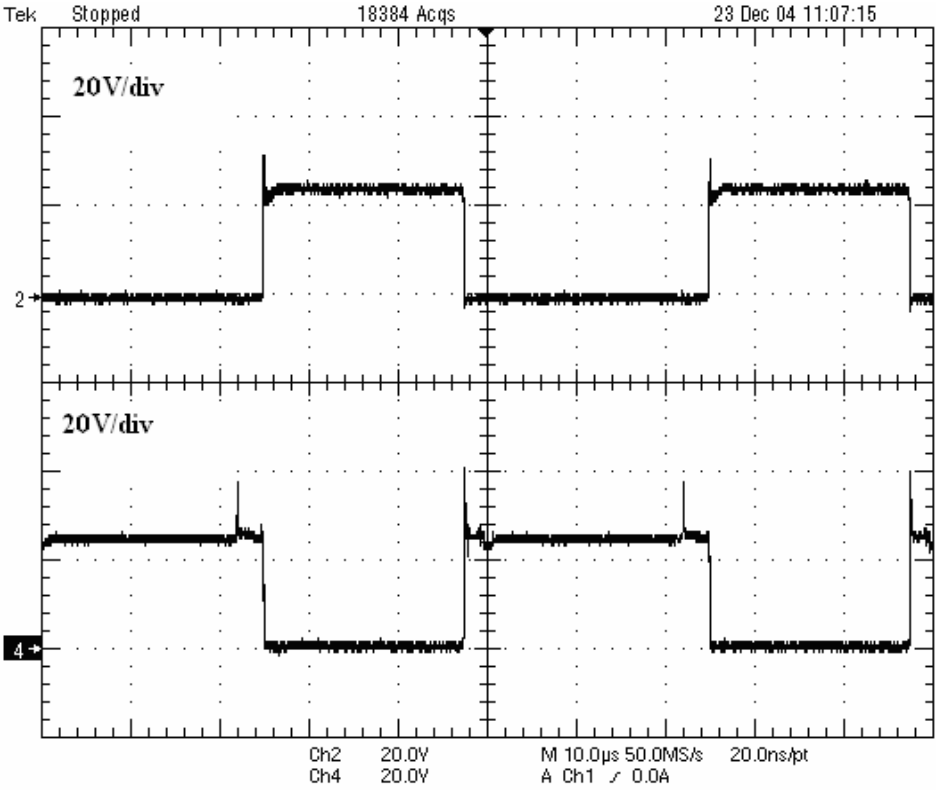

Fig. 17. From Top to Bottom: Experimental Recorded Voltage Across the Upper MOSFET (20V/div) and Across the Lower MOSFET (20V/div) of the Same Leg in the Primary Side with a Time Base of 10us/div

Figure 18 and Figure 19 show the voltage across the MOSFET and the power diode of the same leg in the secondary side, respectively. There are no spikes at all to be seen, which is very good especially at the high (350V) voltage on the secondary side.

The MOSFET and diode both are rated for 600V, and these could be replaced by devices of lower voltage ratings, like 500V and thus the conduction losses could be reduced.

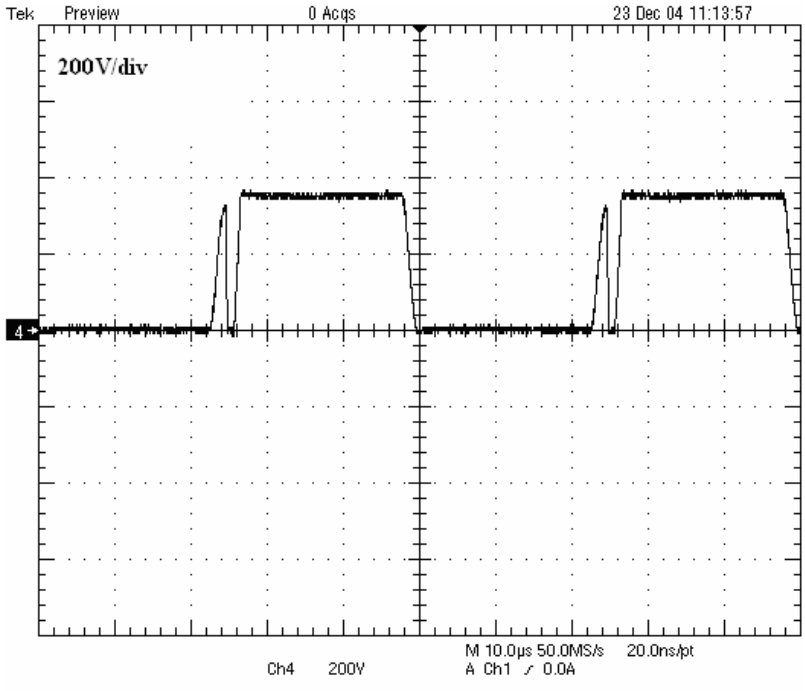

Figure 18. Experimental Recorded Voltage Across the MOSFET (200V/div) in the Secondary Side with a Time Base of 10us/div

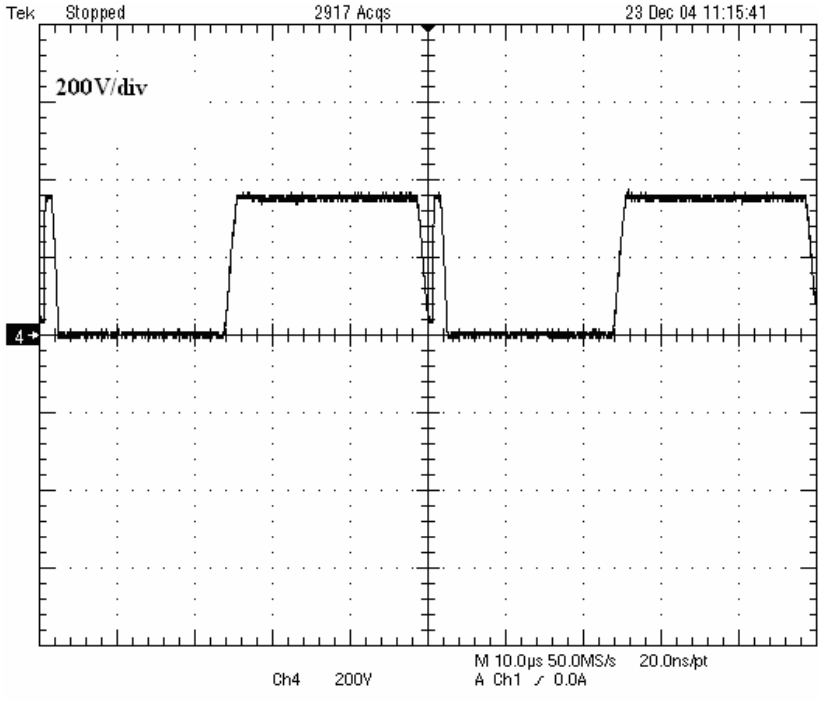

Figure 19. Experimental Recorded Voltage Across the Diode (200V/div) in the Secondary Side with a Time Base of 10us/div

Thus the basic energy transfer principle of the proposed converter is verified experimentally, and the voltage stresses across the power devices are examined, and found to be acceptable. The need for developing a higher power prototype of the proposed converter, while not increasing the ratings of the semiconductor devices by the same proportion, is realized. Therefore an interleaved converter is proposed which is described in the next chapter.

CHAPTER 4

INTERLEAVING

Principle of Interleaving and its Advantages

Interleaving of power converters involves paralleling *n* (>1) individual power converter units to provide *n* times the power of each individual converter. The aim of interleaving power converters is to divide the current flowing through the semiconductor switches (by a factor of *n*), thereby reducing conduction losses and enabling use of lower rated silicon. Interleaving also results in lower amplitudes of input and output current ripple, thereby reducing the size of input and output capacitors. Paralleling semiconductor switches, rather than paralleling the entire units also results in dividing the current flowing through each switch, but it does not reduce the input and output current ripple [24].

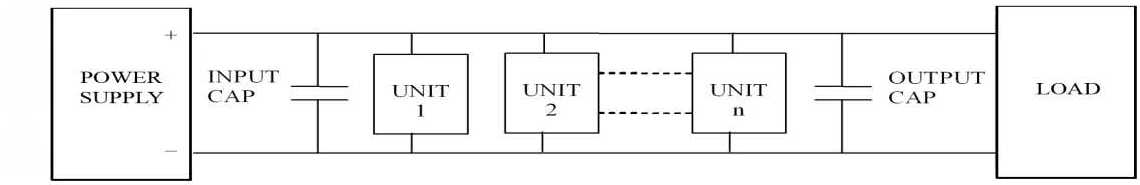

Figure 20. Interleaving of DC-DC Converters

Interleaving *n* DC-DC converter units introduces 360/n phase displacement between high frequency ripples generated by two adjacent phases. The overlap of these displaced or phase-shifted ripples makes their sum flatter. The frequency of the total ripple is n multiple of the frequency of each phase, and the amplitude of the combined

ripple is reduced. An interleaved DC-DC voltage converter for fuel cell applications reduces the ripple amplitude of the high frequency input current, which also helps avoid high frequency interaction inside the fuel cell stack and prolongs fuel cell lifetime [25].

Simulation Schematic and Results

Simulation was run for two interleaved 550W units of the proposed converter delivering a total of 1.1kW of power, with fuel cell input voltage 21-42V and output voltage of 350V. To interleave two units they have to be operated with a phase difference of 90 degrees. The simulation schematic as seen in the PSIM interface is shown in Figure 21. The gating signals (turn on instant and turn off instant) to all the MOSFETs with the required phase delays (in degrees) are marked on the schematic.

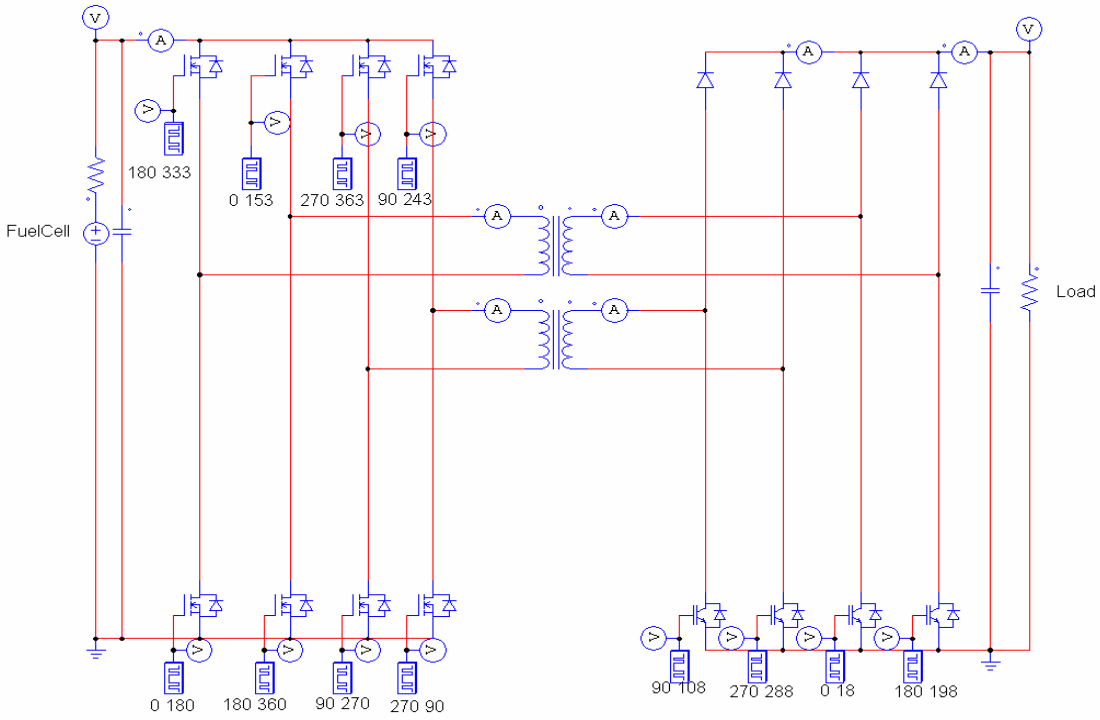

Figure 21. Simulation Schematic of Two 550W Interleaved Units of the Proposed Converter

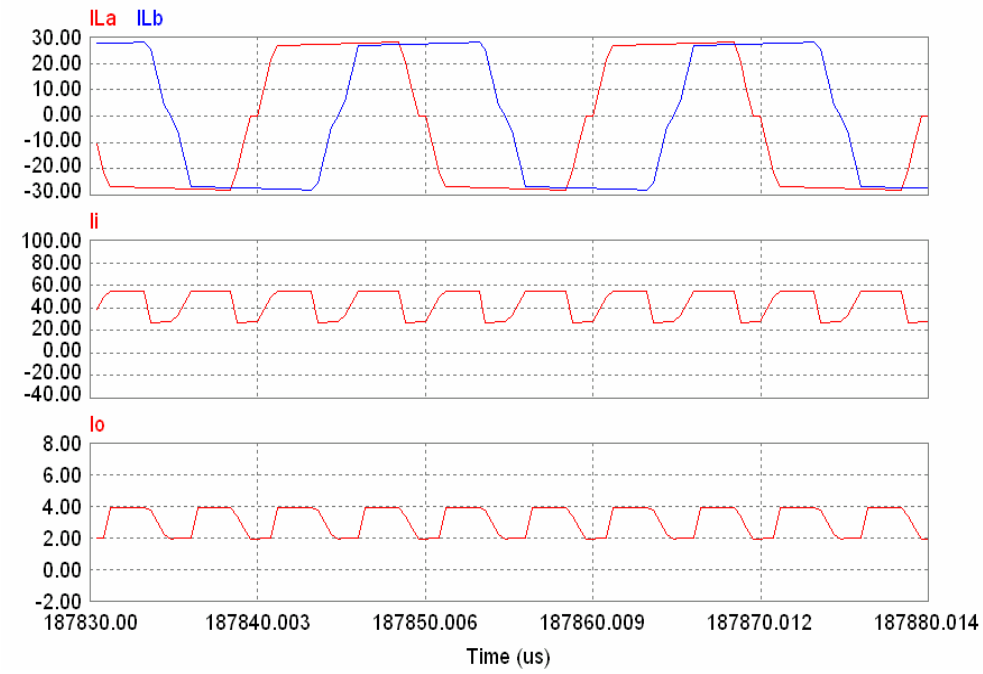

Figure 22. Simulation Results for Two Interleaved 550W Units. From Top to Bottom: Current through the Two Isolation Transformers, Input Current and Output Current

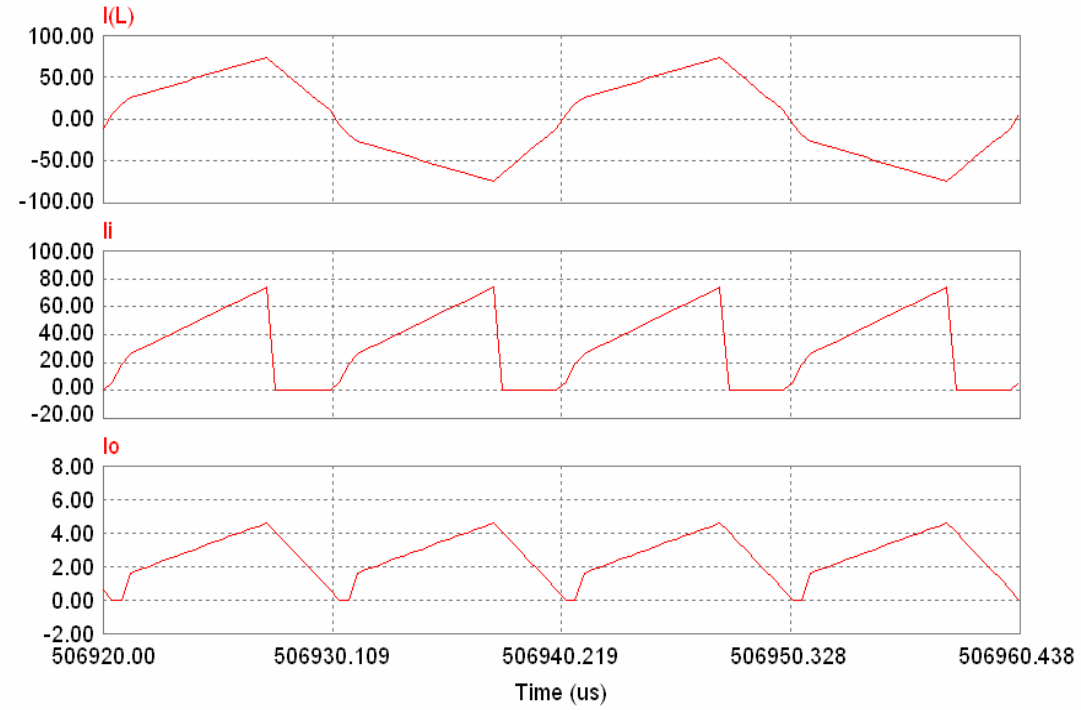

Figure 23. Simulation Results for Stand Alone Single 1.1kW Unit. From Top to Bottom: Current through the Isolation Ttransformer, Input Current and Output Current

The simulation is run for 400ms with a time step of 0.02us to enable generation of high resolution waveforms. Figure 22 shows the simulation results; the two transformer primary current waveforms with a phase shift of 90 degrees, the converter input current and the output current. Figure 23 shows the simulation results for a non-interleaved, stand alone 1.1kW unit of the proposed converter, with 21-42V input fuel cell input voltage and 350V output. By comparing the results of Figure 22 and Figure 23 it can be seen that interleaving two units has resulted in the reduction of the input current ripple peaks from 75A in a stand alone unit to 55A in the interleaved converter. The current ripple in the interleaved unit also has a flattened top as discussed earlier. The output current ripple peak also reduces from 4.5 A to 4A, with the top flattened. This flattening of the current ripple and reduction in amplitude of current ripple peak, results in reduction of size of input and output capacitors, and hence cost of the converter. It also reduces the stresses across the semiconductor devices of the converter.

Experimental Setup

This section describes the experimental setup to interleave two 550W units of the proposed converter to obtain a 1.1kW converter. The schematic of the power train of the converter is shown in Figure 24. Figure 25 is a photograph of the prototype breadboard built in the laboratory. Table 5 lists the cost of the various components on the breadboard, and thus the derived cost per kW.

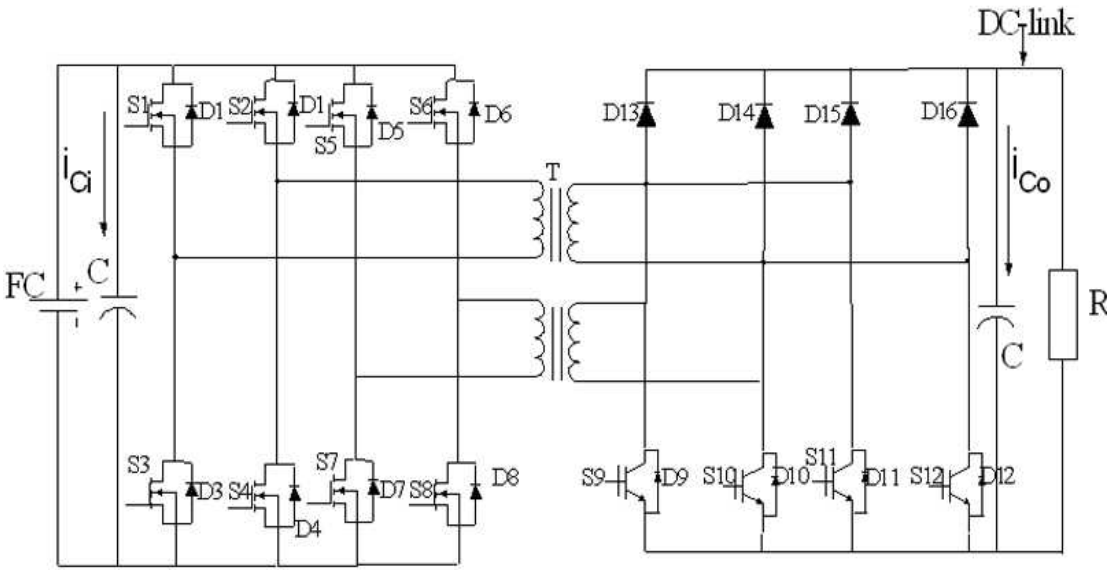

Figure 24. Schematic of Two Interleaved Units of Proposed Converter

Figure 25. 1.1kW Interleaved-Units Prototype Breadboard

Table 5. Material Used in the 1.1kW Interleaved-Unit Prototype Breadboard and Cost of Materials

Key Material	Cost for MSU 1.1 kW prototype ($) (10,000 pieces)	Cost for MSU 5 kW prototype ($) (10,000 pieces)
Power Circuit	34.54	113.73
Devices	8.16	36.72
Capacitors	16.3	31.65
Inductors	-	-
Transformers	2.24	10.08
Other	7.84	35.28
Control Circuit	6.05	27.225
Resistors	1.2	5.4
Capacitors	0.15	0.675
IC's	1.95	8.775
Transistors	1.03	4.635
Signal Transformers	1.72	7.74
Miscellaneous	15.5	65.5
Total	56.09	206.45
Cost per kW	50.99	41.29

Implemented Circuits

UC3525 from Texas Instruments was chosen as the PWM control IC. The UC3525 is a monolithic integrated circuit that includes almost all of the control circuit necessary for a pulse width modulating regulator. Figure 26 shows the pin outs and the internal logic circuit of the UC3525.

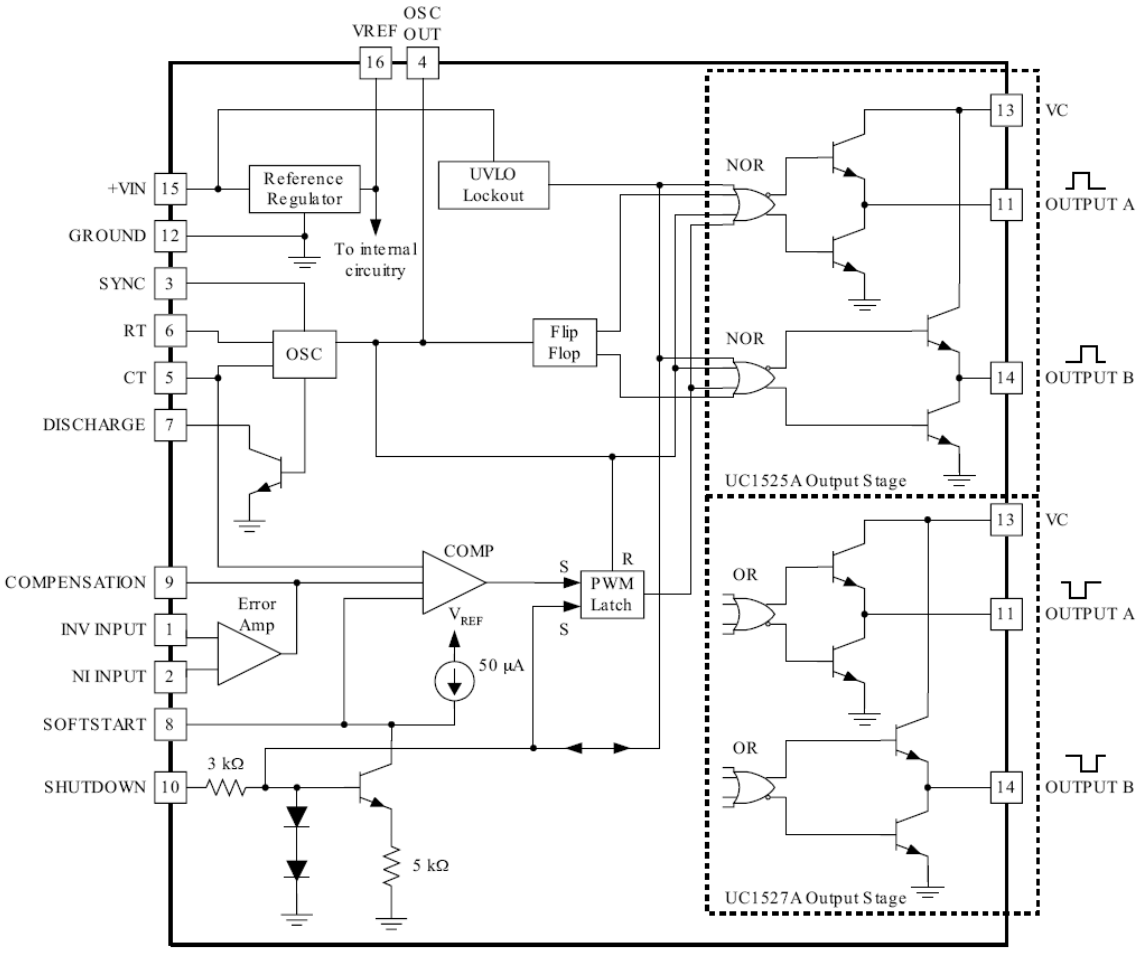

Figure 26. Pin Out and Internal Logic Diagram of UC3525

Pins 1 and 2 are the inverting and non-inverting inputs respectively to the internal error amplifier of the IC. The inverting input is typically connected to a voltage divider resistor network which senses the output voltage level of the power converter. The non-inverting input is connected to a reference voltage used for comparison with the sensed output voltage level. Pins 5 and 6 are connected to the external timing resistor and capacitor respectively that determine the frequency of the internal oscillator of the IC, and thus the frequency of the output PWM signals. Pin 4 gives the output signal of the internal

oscillator. Pin 7 is typically connected to Pin 5 to allow the discharge of the timing capacitor. Pin 16 provides an accurate 5.1 V voltage reference. Pin 13 supplies power to the logic and analog circuitry as well as the internal driver circuitry on the integrated circuit. Pin 12 provides the ground reference, and pins 11 and 14 give the two PWM output signals, 180 degrees out of phase. Pin 3 is used for synchronization and allows a sync input to the oscillator which enables multiple units to be slaved or a single unit to be synchronized to an external system clock.

For a single unit of the proposed three UC3525 ICs are required to generate the six PWM control signals for the six active switches. These three UC3525 ICs need to be synchronized in frequency and phase, and this can be done by designating one IC as the master IC, and connecting its pin 4 (oscillator output) to the pin3 (sync) of the other two ICs.

For two interleaved units of the proposed converter, two groups of the UC3525 ICs, each group consisting of three ICs, are needed. These two groups need to be out of phase by 90 degrees, as this phase difference for two units produces the minimum rms noise. Thus all six UC3525 ICs need to be synchronized to exactly the same operating frequency, but the two groups need to have a phase difference of 90 degrees.

This is achieved by the circuit illustrated with block diagrams in Figure 27, and shown schematically in Figure 28. One UC3525 is used as the master IC, operating at 100 KHz; twice the desired 50 KHz switching frequency of the converter. The two 180 degrees out of phase, 50% duty cycle outputs of the master IC are then each divided in frequency by two. The frequency division is done by the IC 74LS74, which consists of

two edge triggered D-type flip-flops. An edge triggered D-type flip-flop can be configured as a divide by two-counter, by tying the Q-bar output, to the D input. The signal to be divided in frequency by two is fed as the clock signal to the flip flop. The two outputs of the master IC are each thus each divided in frequency by two in the 74LS92, giving two 50% duty cycle signals, out of phase by 90 degrees.

These two signals are then fed to the IC SN74LS122, comprising of two monostable multivibrators. The SN74LS122 is configured using external RC circuit to output pulses of about 500nsecs. These narrow TTL pulses, 90 degrees out of phase, but operating at exactly the same frequency (50 kHz) are connected to the pin 3 (sync) of the UC3525 ICs of the two different groups, as shown in Figure 45 and Figure 54. Thus the two groups of UC3525 ICs are synchronized to the same frequency with a phase lag of 90 degrees.

The 12 generated PWM signals are fed to 6 MOSFET driver ICs, the IR4427 in this case. The IR4427 amplify the PWM signals to the power level needed to enhance the MOSFETS.

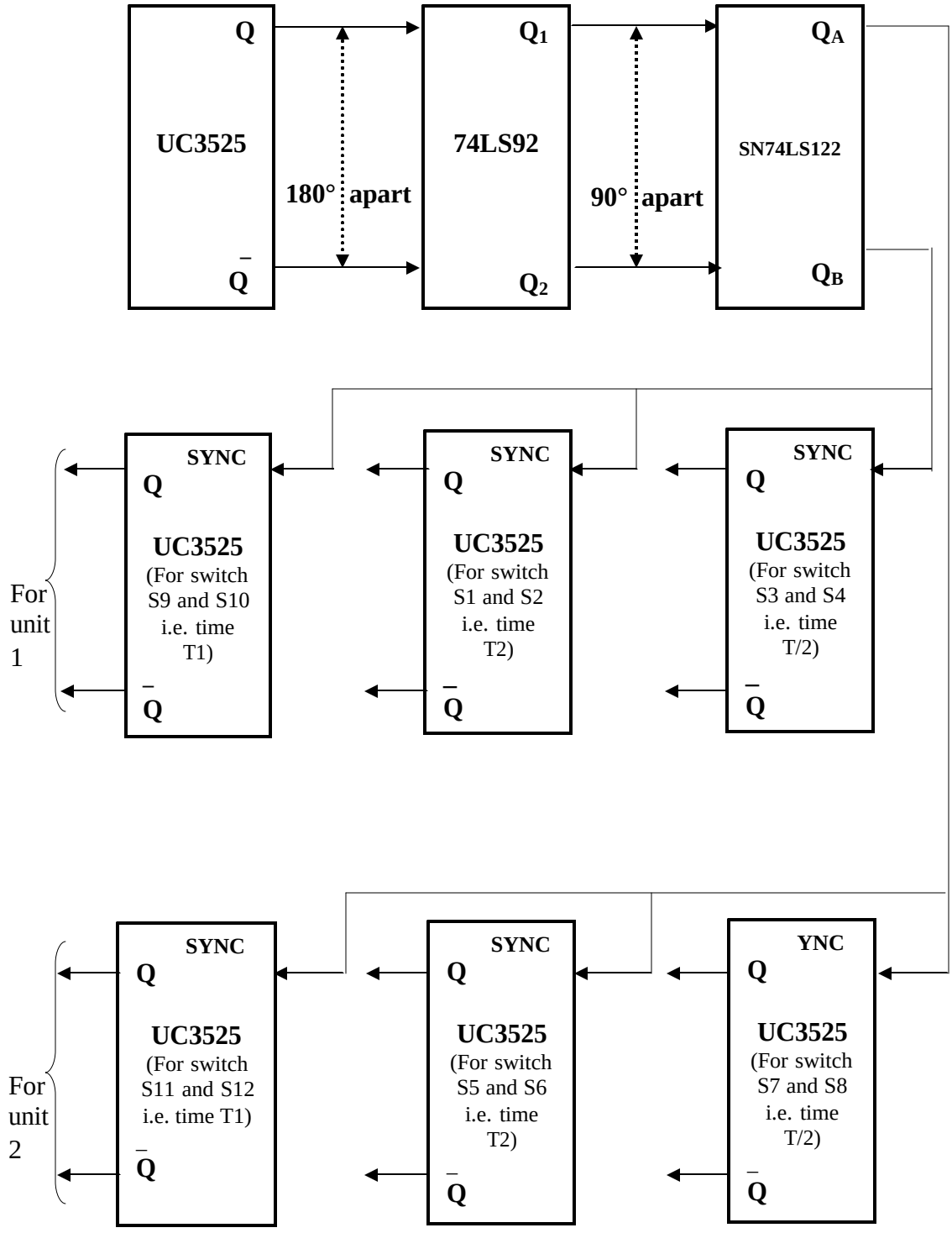

Figure 27. Block Diagram of 90 Degrees Phase Shifting of PWM Signals for the Interleaved Units

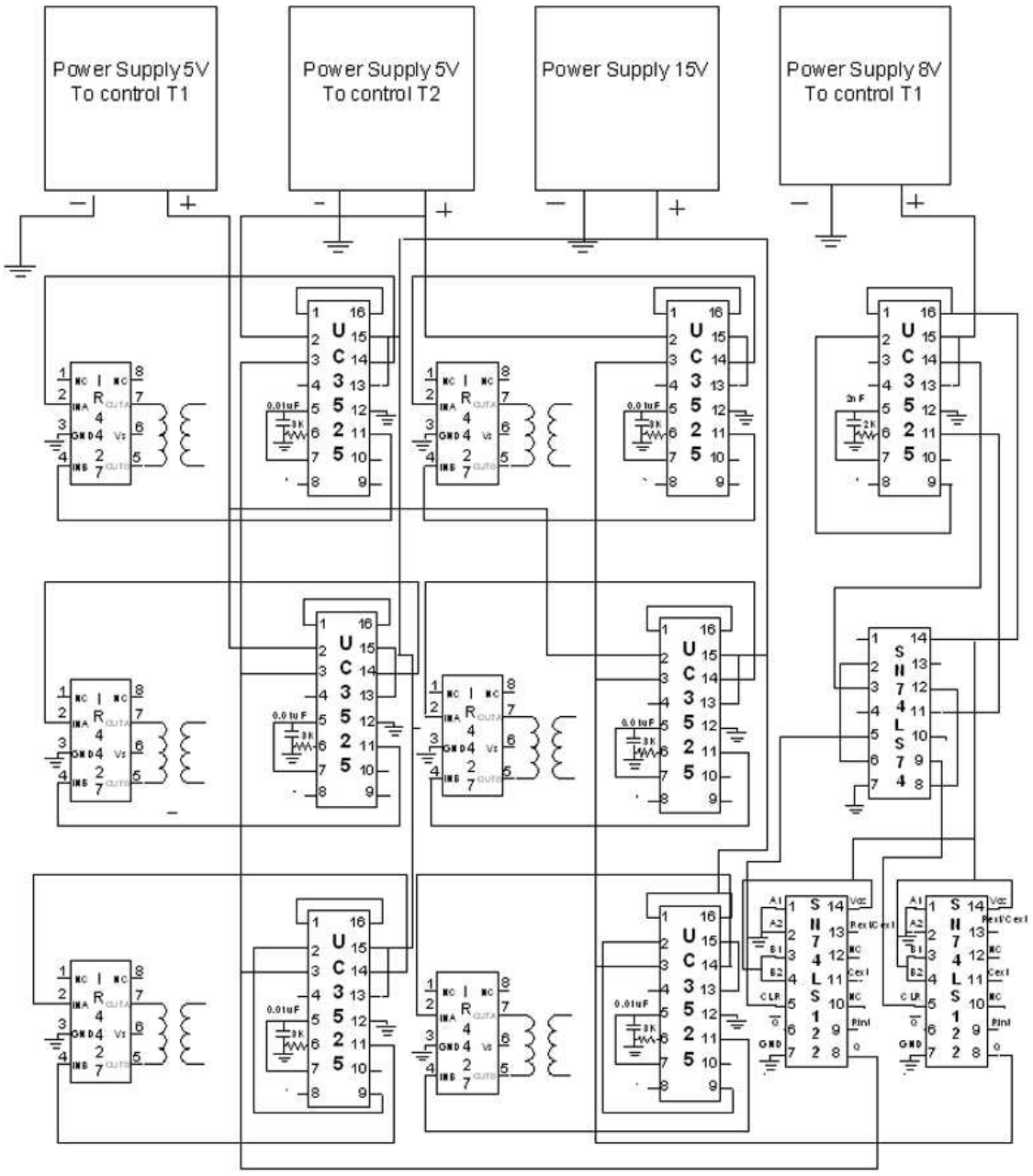

Figure 28. Schematic of 90 Degrees Phase Shifting of PWM Signals for the Interleaved Units

To electrically isolate the output of the converter from the input, no direct electrical connections are made between the primary and the secondary sides of the converter. The

control section of the converter, including the PWM generation, synchronization and the driver circuitry, is on the secondary side of the converter, since the output voltage is inputted into the control section through a resistor divider. Thus the PWM control signals for the MOSFETs on the primary side of the converter need to be electrically isolated from the control circuit. Four transformers are thus used to carry the PWM control signals over the isolation boundary, from the secondary side to the primary side. Thus PWM control signals for all 12 MOSFETs of the two interleaved units are successfully generated and appropriately delivered to each MOSFET.

Figure 29 shows from top to bottom, the PWM control signals of three MOSFETs of the same half cycle of one unit, measured between the drain and source of the MOSFETs and the current through the power transformers of the other unit, at low power (about 50W). It can be seen that the transformer current confirms to the designed scheme of the proposed converter.

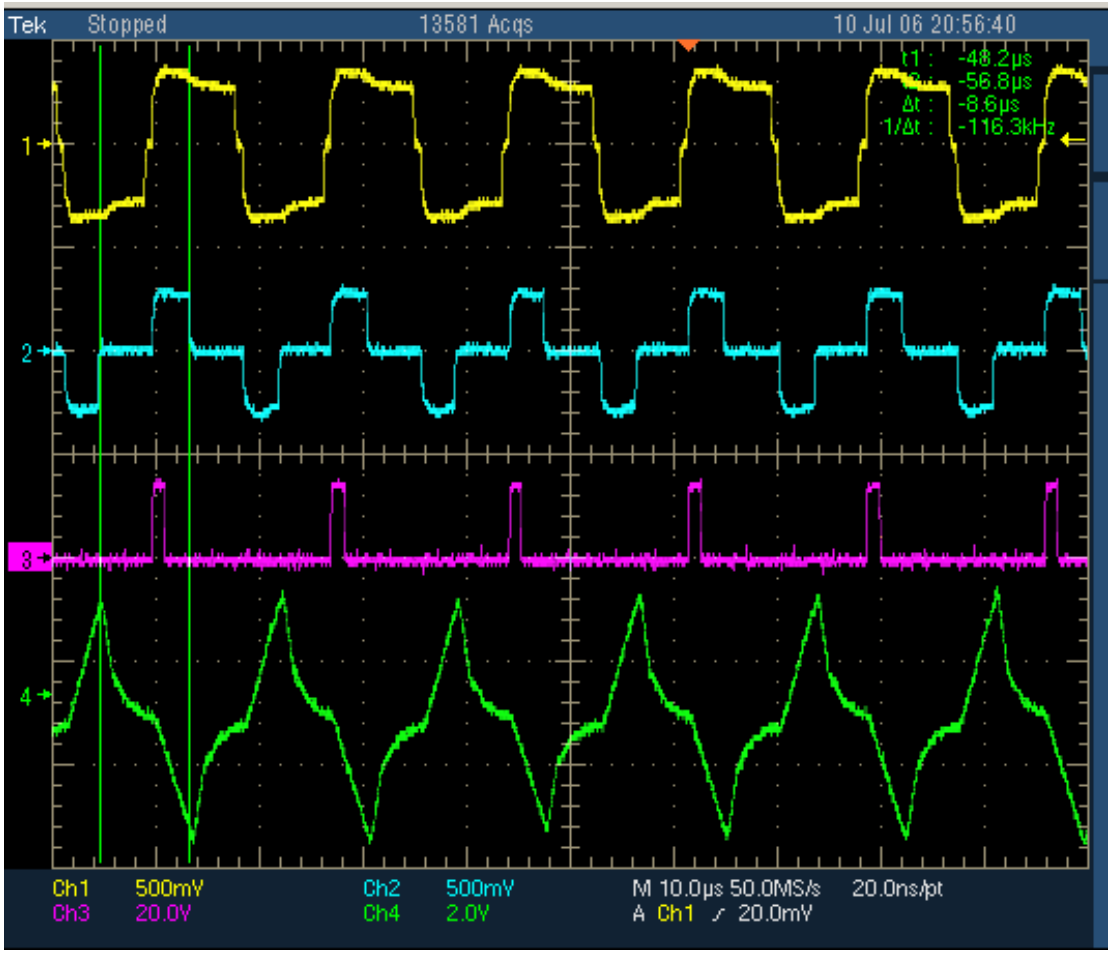

Figure 29. Synchronized, Isolated PWM Control Signals and Transformer Current

Challenges and Recommendations

The UC3525 IC's internal flip flop does not have a reset control. Thus on powering up the IC, either the output A can lead the output B by 180 degrees, or lag the output B by 180 degrees, depending on the flip flop's last state when the IC was turned off; i.e. if the output A at pin 11 of two synchronized UC3525s are seen simultaneously on the oscilloscope, the waveforms would be synchronized in frequency, but can be either be completely in phase or completely out of phase (180 degree phase difference).

This would vary randomly at each power up, and cannot be controlled. Thus in the 90 degrees delay synchronization circuit, the outputs A of the three UC3525 in the same group, were not necessarily always in phase, as outputs A and B of each IC can be exchanged at each instant of power up. For this work, the synchronization signal was manually turned on and off, till the output A of all the ICs aligned with each other in phase.

Since this is an inherent problem of the UC3525, and also of all PWM generation ICs with two outputs, it is recommended that a PWM generation IC with a single output be used. One such IC that can be used is UCC3581 from Texas Instruments. It is priced at $1.00 for large volumes, as compared to $1.05 for the UC3525. But using a PWM generation IC with one output as compared to using a PWM generation IC with two outputs for an application would entail using twice as many numbers of the ICs and therefore would increase the total cost of the converter.

CHAPTER 5

CONCLUSION AND FUTURE WORK

This thesis has presented a unique topology for an isolated DC-DC converter for fuel cell powered distributed residential power generation systems. With dwindling fossil fuel reserves, renewable energy sources like fuel cells are taking the centre stage in the power generation arena, and thus development of affordable, efficient power conditioning systems for fuel cells has become imperative. This thesis work is aimed at contributing towards this effort.

The proposed DC-DC converter utilizes the leakage inductance of the isolation transformer for energy transfer, instead of considering it as a parasite. Thus the proposed converter does not have the problems of reduced efficiency and increased difficulty in control, caused by high leakage inductance.

Simulation and experimental work are done and successful results are presented that verify the energy transfer concept of the proposed converter. Control scheme is proposed for the converter, and successfully simulated, and closed loop simulation results are presented. Interleaving is proposed for the converter, and successful simulation work verifies the advantages of interleaving. Prototype of two 550W interleaved units of the proposed converter is built. Control scheme for generating PWM signals for the two phase shifted units is designed and implemented. Isolation and drive circuitry for the PWM signals is also designed and implemented.

Future Work

A complete power conditioning system for a fuel cell powered distributed residential power generation system, includes a DC-AC inverter following the DC-DC converter to provide regulated AC supply power. Future work could include development of an economical and efficient DC-AC inverter which would result in a complete power conditioning system for such an application. The power level of the laboratory power conditioning system could be scaled higher (<5kW) to emulate closer a fuel cell powered distributed residential power generation system. For this purpose a high power fuel cell or a high power laboratory power-supply could be used.

BIBLIOGRAPHY

1. U.S. Department of Energy, Hydrogen, Fuel Cells & Infrastructure Technologies Program. http://www1.eere.energy.gov/hydrogenandfuelcells/glossary.html.

2. Twidell, J. "Renewable energy: Implementation and benefits," 2nd International Conference on Advances in Power System Control, Operation and Management APSCOM-93, Vol. 1. Hong Kong, Dec 7-10 1993, pp. 418-424.

3. Krist, K., & Gleason, K.J. "SOFC-based residential cogeneration Systems." Electrochemical Society Proceedings 99, Issue 19, pp 107-115.

4. Shipley, A.M. & Elliot, R.N. "Stationary fuel cells: Future promise, current hype." Report Number IE041, American Council for an Energy-Efficient Economy, March 2004.

5. Farooque, M. & Maru, H.C. "Fuel cells-the clean and efficient power generators." Proc. IEEE, Vol. 89, No. 12, pp. 1819–1829, Dec. 2001.

6. Williams, M.C. "Fuel cells and the world energy future." In Proc. IEEE/PES Summer Meeting, Vancouver, BC, Canada, Jul 15–19, 2001, Vol. 1, p. 725.

7. Xu, H., Kong, L. & Wen, X. "Fuel cell power system and high power DC-DC converter power electronics." In IEEE Transactions on Power Electronics, Vol. 19, Isuue %, Sept. 2004, pp. 1250-1255.

8. Fuel Cell Handbook, 6th ed. Washington, DC: U.S. Department of Energy, Nov. 2002, DOE/NETL-2002/1179.

9. Wang, J., Peng, J.A., Anderson, A & Buffenbarger, R. "Low cost fuel cell inverter system for residential power generation." In Proc. IEEE/APEC, Anaheim, CA, Feb. 22–26, 2004, Vol. 1, pp. 337–367.

10. Changrong, L., Johnson, A., & Lai, J-S. "A novel three-phase high-power soft-switched DC/DC converter for low-voltage fuel cell applications. In IEEE Transactions on Industry Applications, Vol. 41, No. 6, November/December 2005, pp. 1691-1697.

11. Hart, D.W. Introduction to Power Electronics, 1st ed. Englewood Cliffs, NJ: Prentice-Hall, 1997, pp. 213–214.

12. Gopinath, R., Kim, S., Hahn, j-H, Enjeti, P.N., Yeary, M.B., & Howze, J.W. "Development of a low cost fuel cell inverter system with DSP control." In IEEE Transactions on Power Electronics, Vol. 19, Issue %, Sept 2004, pp 1256-1262.

13. Gopinath, R. et al., "Development of a low cost fuel cell inverter system with DSP control." In Conf. Rec. Power Electronics Specialists Conference, 2002. PESC02. 2002 IEEE 33rd Annual, Vol. 1, 23-27, June 2002, pp. 309-314.

14. Nergaard, T., Ferrell, J.F., Leslie, Jih-Sheng Lai, "Design considerations for a 48 V fuel cell to split single phase inverter system with ultracapacitor energy storage." In Conf. Rec. Power Electronics Specialists Conference, 2002. PESC02. 2002. In IEEE 33rd Annual, Vol. 4, 23-27, June 2002, pp. 2007–2012.

15. Tuckey, A.M., & Krase, J.N. "A low-cost inverter for domestic fuel cell applications." In Conf. Rec. Power Electronics Specialists Conference, 2002. PESC02. 2002 IEEE 33rd Annual, Vol. 1, 23-27, June 2002, pp. 339 -346.

16. Anderson, G.K, Klumpner, C., Kjaer, S.B., Blaabjerg, F. "A new green power inverter for fuel cells." In Conf. Rec. Power Electronics Specialists Conference, 2002. PESC02. 2002 IEEE 33rd Annual, Vol. 1, 23-27, June 2002, pp. 727 -733.

17. Mazumdar, et al., "High frequency low cost DC-AC inverter design with fuel cell source for home applications." In Conf. Rec. Industry Applications Conference, 2002. 37th IAS Annual Meeting. Conference Record of the, Vol. 2, 13-18 Oct. 2002, pp. 789 -794.

18. Krien, P.T., Balog, R.S., & Geng, X. "High-frequency link inverter for fuel cells based on multiple-carrier PWM. In IEEE Transactions on Power Electronics, Vol. 19, Issue 5, Sept 2004, pp.1279-1288.

19. Dixon, L.H., Jr. "Switching power supply topology review." In Unitrode (TI) Power Converter Seminar SEM300, 1984.

20. Edmunds, M. "Hard switching vs. soft switching." Case study, Xantrex Technologies, Inc. www.xantrex.com/web/id/910/docserve.asp.

21. Watson, R., & Lee, F.C. "A soft-switched full-bridge boost converter employing an active-clamp circuit." In Conference Proceedings of IEEE Transactions on Power Electronics, Vol. 8, No. 4, Oct 1993, pp. 530-534.

22. Mohan, N., Robbins, W., & Undeland, T. Power electronics: Converters, applications and design, 3rd edition, pp. 162-163. John Wiley & Sons, Inc.

23. Whitaker, J.C. (Ed.) The Electronics Handbook. Technical Press, Inc., 1996, p. 1830.

24. Cho, J.G., Sabate, J.A., Hua, G., & Lee, F.C. "Zero-voltage and zero-current-switching full bridge PWM converter for high power applications." In IEEE Transactions on Power Electronics, Vol. 11, Issue 4, July 1996, pp.622-628.

25. Balogh, L., Redl, R., & Sokal, N.O. "A novel soft-switching full-bridge DC/DC converter: Analysis, design considerations, and experimental results at 1.5 kW, 100 kHz." In Conference Proceedings of IEEE 21st Power Electronics Specialist Conference Proceedings of IEEE 21st Power Electronics Specialists Conference 1990, June 1990, pp.162-172.